Chapter 5

Mesoscopic Conductors

The previous chapter is concluded with a rather provocative statement that the inherent noise of a macroscopic conductor is governed by Johnson-Nyguist thermal noise and quantum mechanical zero-point fluctuation even when an internal current flow exists so that a system is not at thermal equilibrium. This is a surprising result, because the equipartition theorem, which is responsible for the thermal noise, can apply only for an equilibrium system. Indeed, if a conductor size decreases and becomes comparable to the electron scattering length, the shot noise normally appears on the dc current. We will show in this chapter how such non-equilibrium transport noise is suppressed when a conductor size is increased.

5.1 Electrons in Mesoscopic Two Dimensional Systems

For mesoscopic conductors, the length scale is inbetween microscopic and macroscopic systems, and bounded on one side by the deBroglie wavelength of the electron, and on the other, by the length scales for various scattering mechanisms that destroy the electron's phase coherence or momentum. A modulation doped, gallium arsenide two-dimensional electron gas (GaAs-2DEG) is one system where devices can be fabricated to have dimensions satisfying these requirements. A Ferm degenerate 2DEG is formed in the triangular potential well created by charge transfer in the z direction at the interface between non-doped GaAs and doped AlGaAs as shown in Fig. 5.1[1, 2].

The electron dynamics on the mesoscopic scale can be well approximated by an envelope function satisfying the effective mass equation. This Schrödinger-like equation forms the mathematical foundation for mesoscopic electron transport. The exact Schrödinger wavefunction, Φ, can be found in the independent electron approximation (which ignores electron-electron interactions) by solving the single particle Schrödinger equation,

$$i\hbar \frac{\mathrm{d}}{\mathrm{d}t}\Phi = H\Phi, \qquad H = \frac{\mathbf{p}^2}{2m_\mathrm{e}} + V(\mathbf{r}, t) \quad , \tag{5.1}$$

where m_e is the free electron mass, and $\mathbf{p}$ and $\mathbf{r}$ are the momentum and position operators. In general, the potential, $V(\mathbf{r}, t)$ seen by the 2DEG electrons includes the periodic lattice potential, $V_\mathrm{l}(\mathbf{r})$, its time-dependent fluctuations (phonons), $V_\mathrm{ph}(\mathbf{r}, t)$, the electrostatic confinement potential, $V_\mathrm{e}(\mathbf{r})$, and the random disorder potential, $V_\mathrm{d}(\mathbf{r})$, due to various defects and impurities.
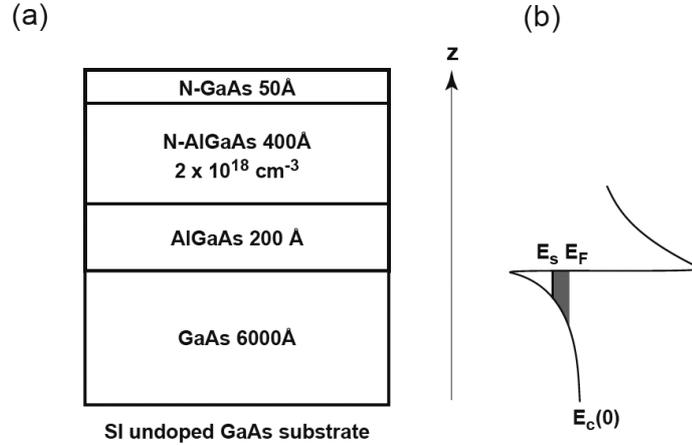
Figure 5.1: (a) The epitaxial structure of a GaAs-2DEG. (b) Conduction band energy diagram near the interface between the non-doped GaAs and AlGaAs. A two dimensional electron gas forms in the triangular well.

Starting with just the periodic potential, the structure of the electron's wavefunction and energy would generally be found using Bloch's theorem[3]. This theorem states that the exact wavefunctions of a static periodic potential can be described as the product of a plane wave of wavevector $\mathbf{k}$ and a periodic function,

$$\Phi_{n\mathbf{k}}(\mathbf{r}) = u_{n\mathbf{k}}(\mathbf{r}) \exp(i\mathbf{k} \cdot \mathbf{r}) \quad , \tag{5.2}$$

where $u_{n\mathbf{k}}(\mathbf{r})$ has the same periodicity as the lattice potential. Here, n is the band index which labels the discrete set of periodic functions that satisfy the Schrödinger equation subject to periodic boundary conditions.

Since this is a fairly difficult problem to solve, and since in practice, only the regions near the minimum of the conduction band at the Brillouin zone center are important for electron transport in the GaAs 2DEG, several simplifying assumptions can be made. Because $\mathbf{k}$ is small in this region, a $\mathbf{k} \cdot \mathbf{p}$ expansion in the Schrödinger equation can be made around the known Bloch wavefunctions and energies at the zone center[4, 5]. From symmetry arguments on the periodic potential, it can be shown using second-order time independent perturbation theory that the conduction band energy depends quadratically on the wavevector,

$$E_{\mathrm{c}}(\mathbf{k}) = E_{\mathrm{c0}} + \frac{\hbar^2 \mathbf{k}^2}{2m} \quad , \tag{5.3}$$

where c has been substituted for n to indicate the conduction band with an effective mass, $m = 0.067 m_{\mathrm{e}}$, that depends on the energy gap between conduction and valence bands, and the dipole moments for the zone center Bloch wavefunctions. Moreover, the functions $u_{n\mathbf{k}}(\mathbf{r})$ can also be expanded in terms of the zone center Bloch wavefunctions, and possess a term linear in $\mathbf{k} \cdot \mathbf{p}$.

Within this approximation, it appears that the energy of the electron can be decomposed into two portions – a constant potential energy term E_{c0} due solely to the band

2

structure, and a parabolic kinetic energy term $\frac{\hbar^2 k^2}{2m}$ due to the plane wave propagation. Through the effective mass, this latter term implicitly includes the effect that the periodicity has on the inertia of the free electron.

Now if a nonperiodic potential is added (e.g., the confinement potential), the time-independent single-particle Schrödinger equation,

$$\left[\frac{\hat{\mathbf{p}}^2}{2m_e} + V_l(\hat{\mathbf{r}}) + V_e(\hat{\mathbf{r}}) \right] \Phi(\mathbf{r}) = E\Phi(\mathbf{r}) \quad , \tag{5.4}$$

where E is the new energy eigenvalue, can be solved by using the Bloch functions as an expansion basis,

$$\Phi(\mathbf{r}) = \frac{1}{\sqrt{\Omega}} \sum_{n,\mathbf{k}} c_{n,\mathbf{k}} u_{n\mathbf{k}}(\mathbf{r}) \exp(i\mathbf{k} \cdot \mathbf{r}) \quad , \tag{5.5}$$

where Ω is the normalization volume. If the reasonable assumption is made that the nonperiodic potential varies slowly in space as compared to the periodic lattice of the atomic scale, then it can be shown using Eq. (5.3) that the Schrödinger equation gives rise to the single band effective mass equation[6, 7],

$$\left[\frac{\hat{\mathbf{p}}^2}{2m} + V_e(\hat{\mathbf{r}}) \right] \Psi(\mathbf{r}) = E\Psi(\mathbf{r}) \quad , \tag{5.6}$$

for the effective mass wavefunction (or the envelope of the Bloch functions),

$$\Psi_n(\mathbf{r}) = \frac{1}{\sqrt{\Omega}} \sum_{\mathbf{k}} c_{n,\mathbf{k}} \exp(i\mathbf{k} \cdot \mathbf{r}) \quad . \tag{5.7}$$

In other words, if coefficients $c_{n,\mathbf{k}}$ can be found so that $\Psi_n(\mathrm{r})$ satisfies the effective mass equation, (5.6), then the exact wavefunctions (within the $\mathbf{k} \cdot \mathbf{p}$ approximation) are given by (5.5).

The advantage of (5.6) is that now all details about the atomic scale periodicity are taken into account by the effective mass, m, leaving only a Schrödinger-like equation to describe the behavior of the plane wave envelopes of the Bloch functions to the slowly varying potentials. The removal of the periodic portions of the Bloch wavefunctions reflects the fact that, to this order of approximation, there are two very different length scales over which the wavefunction varies – rapid variations on the order of the lattice spacing occur for $u_{n\mathbf{k}}(\mathbf{r})$, and slow variations on the scale of $2\pi/k$ for the plane wave. The slowly varying potentials only affect the latter, a point which can usually be verified by the same second-order perturbation theory mentioned above. With this in mind, throughout the remainder of this chapter, the effective mass approximation will be assumed, and any reference to an "electron" refers to the effective mass wavefunction rather than the exact wavefunction.

If the z direction confinement potential is translationally invariant in the lateral direction, a separation of the conduction band wavefunctions, $\Psi_c(\mathbf{r})$ from (5.7), into a standing wave in the z direction and plane waves in the lateral directions is possible. Now the energy can be written as

$$E(\mathbf{k}) = E_c(0) + E_s + \frac{\hbar^2 \mathbf{k}^2}{2m} \quad , \tag{5.8}$$

3

where E_s is the confinement energy along z direction (subband energy), and $\mathbf{k}$ from now on refers to the 2D lateral wave vector.

For the electron dynamics within this well, a wave packet centered around a particular value of $\mathbf{k}$ can be constructed which would then be evolved by the time-dependent version of the effective mass equation. From Eq. (5.8), the group velocity of this wave packet is just

$$\mathbf{v}(\mathbf{k}) = \frac{1}{\hbar}\nabla_{\mathbf{k}}E(\mathbf{k}) = \frac{\hbar\mathbf{k}}{m} \quad . \tag{5.9}$$

Here, $\hbar\mathbf{k}$ is recognized as the crystal momentum which represents the momentum of the wave packet moving between many unit cells (in contrast to the real momentum, which is dominated mainly by the motion of the free electron wave packet within a unit cell). Throughout the remainder of this chapter, momentum will be used to refer to the crystal momentum as long as the effective mass equation is valid.

Thus far, only a single electron has been considered. In a 2DEG though, there is a degenerate gas of two dimensional plane wave electrons. At low temperatures, Θ, Fermi-Dirac statistics are appropriate, giving an average occupation per energy of $f(E) = f_{\mathrm{FD}}(E)$. The density of states per subband of the well (including spin degeneracy) can be derived from (5.8),

$$\rho_{\mathrm{2D}}(E) = \frac{m}{\pi\hbar^2} \quad , \tag{5.10}$$

and is independent of energy. The sheet density, n_s, can be found by integrating the product of this density of states with the Fermi-Dirac distribution function, yielding a sheet density proportional to the Fermi energy. For a GaAs-2DEG, this is typically on the order of $10^{11} \sim 10^{12}$ cm^{-2}. Moreover, for densities below approximately 7×10^{11} cm^{-2}, usually only the lowest subband of the well is occupied.

Because of the degenerate nature of the electrons, the conductance properties are determined mainly by the electrons at the Fermi energy. In contrast, in the classical theory of conduction by Drude, which assumes a Maxwell-Boltzman distribution of electrons, there is a contribution from all of the electrons. In the degenerate case, the electrons near the Fermi surface only contributes to net transport and have the Fermi wavelength (deBroglie wavelength),

$$\lambda_{\mathrm{F}} = \frac{h}{p_{\mathrm{F}}} = \sqrt{\frac{2\pi}{n_{\mathrm{s}}}} \quad , \tag{5.11}$$

which is around 40 nm in a GaAs 2DEG. Here $p_{\mathrm{F}} = \hbar k_{\mathrm{F}}$ is the electron momentum at a Fermi energy.

5.2 Ballistic Transport

5.2.1 Conductance Quantization

It is possible to produce devices with a length and width smaller than the momentum relaxation length (mean free path). In this regime, the transport is ballistic. If the phase relaxation length is also longer than the device dimensions, then the transport is clearly coherent.

Electron waveguides are essentially wires narrow enough (on the order of the deBroglie wavelength) that the electron wavefunction must be quantized in the transverse dimension.

The simplest realization of this is the quantum point contact (QPC), shown schematically in Fig. 5.2. In the QPC, the 1D subbands are widely spaced (uniformly if the confining potential is parabolic). For each subband, the energy of the 1D electrons is given by

$$E_j(k) = E_j(0) + \frac{\hbar^2 k^2}{2m} \quad , \tag{5.12}$$

where $E_j(0)$ is the confinement subband energy and k is now the longitudinal wavevector. The quadratic term generally leads to spreading in the wave packets of electrons as the different waves propagate at different speeds. Practically though, in the electron case, for small energy changes compared to the Fermi energy, this is usually ignored.
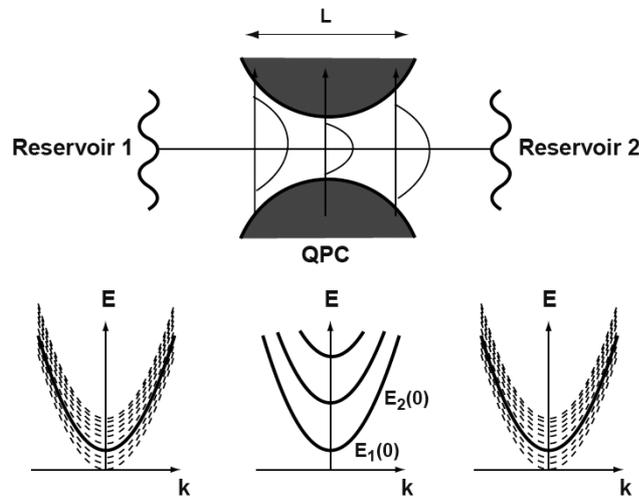

Figure 5.2: A schematic of a quantum point contact (QPC) of nominal length L, connected to large electron reservoirs. The first transverse mode propagates through the point contact. Because of the small dimension, the discrete modes, $E_j(0)$ are well separated. In contrast, in the reservoirs, a large density of modes exists, usually one of which is mode-matched to the QPC.

For transport through this device to occur, it must be connected to contacts which inject electrons. The only available source for electrons in this case is a degenerate, thermal reservoir of electrons in the contacts. Like the QPC, a finite size contact has transverse modes, but since its very large, the number of transverse modes is correspondingly large as depicted schematically in Fig. 5.2. All of these modes are assumed to be identically populated with electrons according to the Fermi-Dirac function with a common chemical potential, μ. We assume that for a given energy below the chemical potential, all of the modes have exactly the same number of electrons, which is simply unity due to the Pauli exclusion principle (or two if spin degeneracy is included). This property is called Fermi-degeneracy.

Electronic conduction between the contact reservoirs is determined by treating the transport through the device as a transmission problem. This idea was first formulated

by R. Landauer[10] for a chain of scatterers between two leads. Only the transmission characteristics of the electrons at the Fermi energy are important. In the independent electron approximation, this transmission can be found by assuming an incident electron state and solving the effective mass equation with the device's electrostatic potential.

Qualitatively, in the case of the QPC, if the Fermi energy is below the lowest subband level, E_1, then the device is pinched off: the transmission, T, goes to zero. If the QPC width is widened so that the subband level drops with respect to the Fermi energy, a finite transmission can be allowed because the evanescently decaying wave may leak through the barrier. Then, when the subband energy drops below the Fermi level, the transmission for electrons at the Fermi level approaches unity if the potential variation over an electron Fermi wavelength $\lambda_F = \frac{2\pi}{k_F}$ is small, as shown in Fig. 5.3.
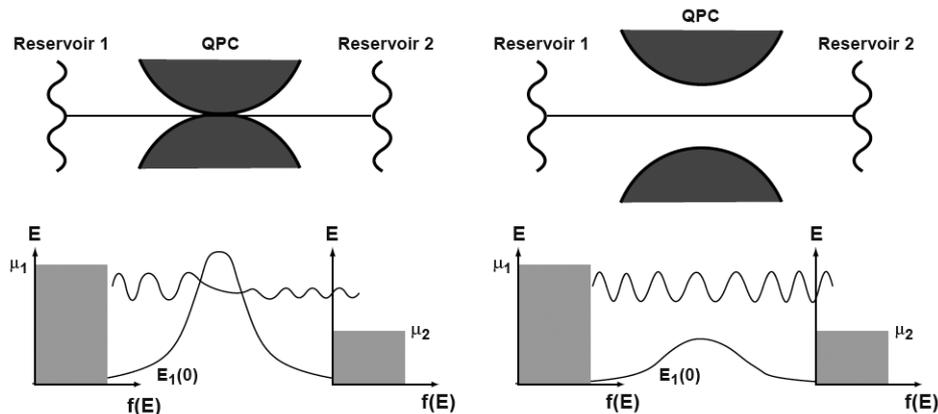

Figure 5.3: (a) QPC near pinchoff. The plane wave electron decays evanescently through the barrier, giving only a small transmission. (b) Open QPC. The subband level is now below the Fermi level so that all electrons can be transmitted with unity probability.

Unity transmission through the device, however, does not imply zero resistance. First, there can still be considerable reflection at the interface between the device and the reservoirs which are the sources and sinks for the electrons. Usually, the transitions at the interfaces occur adiabatically; electrons in the transmitting mode can propagate out of the device into the sink contacts with little reflection[11]. However, most electrons propagating from the source reservoir into the device are reflected, unless they are properly mode-matched with the transverse mode in the QPC.

Second, even for this mode, the current is limited by the Pauli exclusion principle. If a bias is applied between the reservoir chemical potentials, i.e. $\mu_1 = \mu_2 + eV$, then (concentrating only on the states above μ_2 which contribute to net current) the net current in reservoir 2 is given by the transmitted flux from reservoir 1,

$$I_2 = \frac{2e}{h} \int_{\mu_2}^{\mu_2 + eV} dE \rho_{1D}(E) v(E) T f_1(E) \qquad (5.13)$$

$$= \frac{2e}{h}eVT \tag{5.14}$$

since only a single electron is allowed per state per spin. Note the fact that the group velocity $v(E) = \frac{1}{\hbar}\frac{dE}{dk} = \hbar k/m$ and the density of states, $\rho_{1D} = \frac{1}{L}\frac{dN}{dE} = \frac{1}{2\pi\hbar v(E)}$, cancels in 1D permits a straightforward integration of the degenerate term Dirac distribution function. This results in a conductance of

$$G = 2G_Q T \quad , \tag{5.15}$$

where

$$G_Q = \frac{e^2}{h} \tag{5.16}$$

is the quantum unit of conductance, determined only by fundamental constants. The factor of two arises because of spin degeneracy. This is the Landauer formula for the conductance in terms of transmission through a single mode. The heat dissipation associated with it does not occur in the QPC since there is no inelastic scattering there. Instead, it occurs in the reservoirs, and can be attributed to the inelastic processes which relax the reflected electrons at the input interface, and the transmitted electrons at the output.
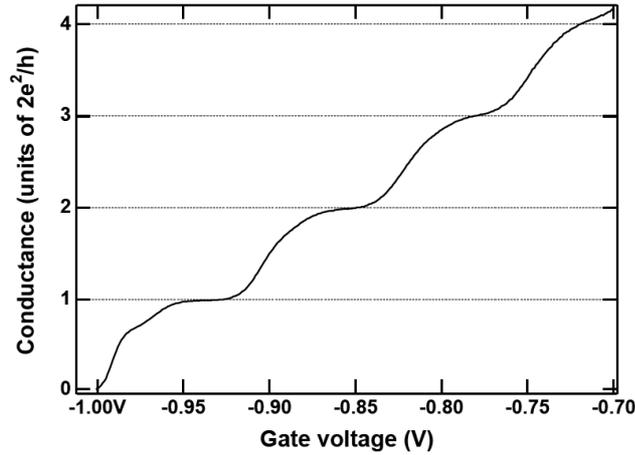

Figure 5.4: The conductance of a QPC vs. the gate voltage. The conductance is quantized in units of $2e^2/h$. At each plateau, all electrons injected into the transmission modes without reflection contribute to the conductance. At each step, the transmission probability of the highest transverse mode transitions from zero to unity.

Experimentally, this quantized conductance was first observed in 1988, in the GaAs 2DEG system[12, 13]. Besides the first plateau, additional plateaux can be observed as the channel width increases to allow more transverse modes to propagate. In this case, the conductance is expressed by the multimode formula,

$$G = \frac{2e^2}{h}\sum_j T_j \quad , \tag{5.17}$$

7

where T_j are the transmission probabilities for each mode. This results in steps in the conductance of a fundamental magnitude $2e^2/h$ each time the transmission for each transverse mode transitions from zero to unity (Fig. 5.4)[14].
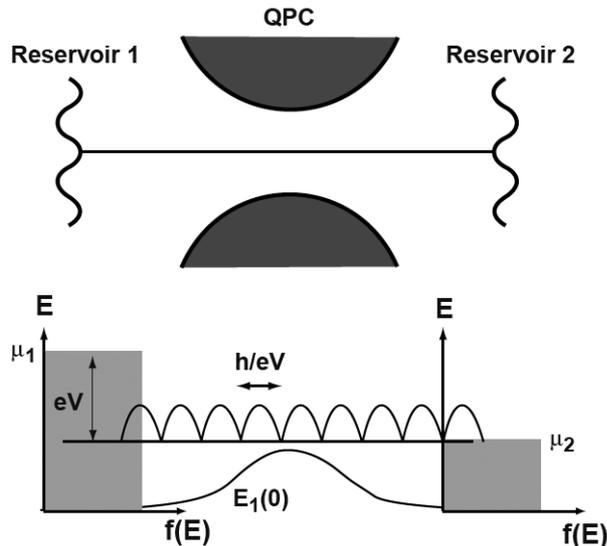

Figure 5.5: The wave packet picture of ballistic transport. An energy bias of eV injects wave packets of nominal time width h/eV into the QPC. Because of the zero temperature Fermi-Dirac distribution, the injection is quiet.

Although this discussion focuses on the longitudinal plane wave states, wave packets can have easily be constructed as well, as shown in Fig. 5.5. This viewpoint is perhaps more natural when considering the particle nature of the ballistic transport. A voltage drop eV across the QPC represents the range of electron energies which can contribute to the wave packet construction. In the simplest picture, at zero temperature, the Fermi-Dirac distribution restricts wave packets to a width of $\frac{h}{eV}(\approx 41$ ps for 100μV$)$. Again, because of the Pauli exclusion principle, each wave packet only accomodates a single electron per spin. These packets are then regularly injected into the QPC for every $\tau = \frac{h}{eV}$ seconds, and coherently transmitted or reflected. Once absorbed into one reservoir or the other though, the wave packets can be considered to be either transmitted or reflected, just like classical billiard balls, resulting in the current $I = \frac{2e}{\tau}T = \frac{2e^2}{h}VT$.

5.2.2 Current Noise at Thermal Equilibrium

Thus far, the focus of the discussion has been on the averaged transport properties of electronic devices in the mesoscopic regime. The Landauer approach has proved to be a very successful paradigm for this. However, it does raise a few questions in relation to noise. As is well known from the Fluctuation-Dissipation Theorem, any dissipation from a system to a reservoir should be associated with a fluctuation injected into the system from the reservoir at equilibrium[15]. In fact, from linear response theory, it is possible to

derive a relationship between the fluctuating properties of a system and the response of the system to external perturbations. The generalized Johnson-Nyquist noise is exactly this kind of relation, as we have seen in the previous chapter.

In the case of mesoscopic devices, the Landauer formula implies that a ballistic conductor with transmission, $T = 1$, has a linear response conductance of G_Q. The conductor should therefore exhibit fluctuations in its current at equilibrium. However, since this dissipation is associated with processes in the reservoir rather than the conductor itself, there is some ambiguity concering how these fluctuations should be interpreted. An elegant picture for this emerges from the wave packet point of view[16].

From this perspective, the electron reservoir is coupled to a thermal bath with which energy can be exchanged to maintain the equilibrium Fermi-Dirac distribution for the electrons. At zero temperature, due to the unity occupation, all wave packets associated with energies below the chemical potential are always occupied, while those above the Fermi energy are always unoccupied. At finite temperature, though, within the approximate width $k_B\Theta$ of the Fermi energy, the average occupation changes from zero to unity. This implies that some of the wave packets are partially occupied.

At thermal equilibrium, both reservoirs of a ballistic conductor are identical so that no net transport occurs. However, each reservoir can be envisioned as independently injecting these wave packets into the conductor in different directions. Since each travelling wave packet carries an electron flux consitituting a current, the statistical, thermal fluctuations in the occupations result in equilibrium current fluctuations.

Consider the one-dimensional mesoscopic conductor (Fig. 5.6), in which electrons propagate from one electrode to the other without being scattered (ballistic transport). The electron emission process from each reservoir electrode obeys a binomial distribution with the average emission rate $f(E)$.
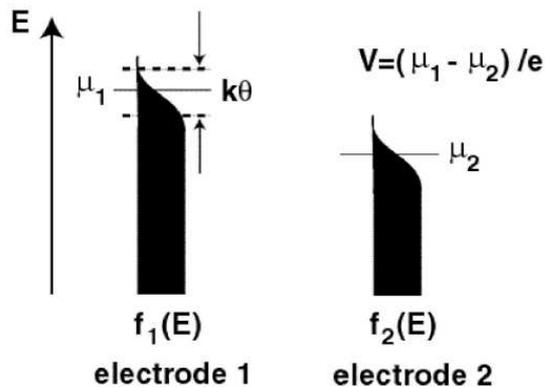

Figure 5.6: One-dimensional mesoscopic conductor at thermal equilibrium.

The electron occupation number in each longitudinal mode with energy E and wave vector k in the reservoir is given by the Fermi-Dirac distribution. We can think of the Fermi-Dirac distribution as a *probability distribution* describing the probability of an electron occupying a propagating mode accross the mesoscopic conductor. The Fermi-

Dirac distribution of electrode 1 (Fig. 5.6) is given by:

$$f_1(E) = \frac{1}{e^{(E-\mu_1)/k_\mathrm{B}\theta} + 1} \quad , \tag{5.18}$$

where μ_1 is the chemical potential (Fermi energy) at electrode 1, k_B is the Boltzmann constant, and θ is the temperature. For each longitudinal mode, the wavevector is quantized to

$$k_\mathrm{N} = \frac{2\pi}{L} N \quad , \tag{5.19}$$

where N is a positive integer and L is the length of the conductor in the direction of transport. The number of modes per unit energy interval centered at an energy E is called the *mode density*, and is given by:

$$D(E) = \frac{dN(E)}{dE} = \frac{dN(k_\mathrm{N})}{dk_\mathrm{N}} \frac{dk_\mathrm{N}}{dE} = \frac{L}{2\pi} \frac{1}{\hbar v_\mathrm{N}(E)} \quad , \tag{5.20}$$

where the relations

$$\frac{dN}{dk_\mathrm{N}} = \frac{L}{2\pi} \;,\; E = \frac{\hbar^2 k_\mathrm{N}^2}{2m} \quad \text{and} \quad v_\mathrm{N} = \frac{\hbar k_\mathrm{N}}{m} \quad ,$$

are used. Here, v_N is the group velocity of the plane wave electron. We also assume that L is large enough that we can take $D(E)$ to be a continuous function.

Current is defined as the number of charges per unit time entering (or leaving) the conductor. Here, each charge travels at a velocity, v_N, over a length L. Thus, for a given mode, the transit time of an electron is $T_R = L/v_\mathrm{N}$, and consequently, the number of charges per second is v_N/L. To get the current carried by a given longitudinal mode, we must multiply by the Fermi-Dirac distribution, which is essentially the probability that an electron enters a given mode. Lastly, to get the total current, we integrate over the current per mode times the number of modes per energy over all energy range. Therefore, the total current from electrode 1 (to electrode 2) is:

$$
\begin{aligned}
I_1 &= 2 \int_0^\infty (dE) \left[\frac{e}{T_R} \right] \cdot f_1(E) \cdot D(E) \\
&= 2 \int_0^\infty (dE) \left[e \frac{v_\mathrm{N}(E)}{L} \right] \cdot f_1(E) \cdot \frac{L}{2\pi\hbar v_\mathrm{N}(E)} \\
&= \frac{2e}{h} \int_0^\infty (dE) \frac{1}{e^{(E-\mu_1)/k_\mathrm{B}\theta} + 1} \quad .
\end{aligned}
\tag{5.21}
$$

Similarly, the current from electrode 2 (to electrode 1) is,

$$I_2 = \frac{2e}{h} \int_0^\infty (dE) \frac{1}{e^{(E-\mu_2)/k_\mathrm{B}\theta} + 1} \quad . \tag{5.22}$$

The net current is $I_\mathrm{tot} = I_1 - I_2 = 0$ for $\mu_1 = \mu_2$, as it should be. We can make the following interpretations:

i) $e/h \; (dE)$ is the contribution to the current by all the longitudinal modes in the energy band $[E, E + dE]$ for a given spin.

ii) $f(E)$ is the probability that the modes in the band $[E, E + dE]$ are filled.

iii) The total current is given by the sum of the contributions over all energies.

Using this interpretation, the power spectral density (PSD) at zero frequency limit can be found from the variance for such a random partition process [Carson theorem in chapter 1]. The probability of electron emission is $f(E)$, and the variance is thus $f(1 - f)$. This essentially becomes a binomial problem. The noise PSD for the energy band $[E, E + dE]$ is given by:

$$
\begin{aligned}
S_{I_1}(\omega = 0)dE &= 2\nu \langle \Delta a^2 \rangle |F(i\omega \simeq 0)|^2 \\
&= 2 \cdot \frac{2dE}{h} \cdot e^2 f_1(E) \left[1 - f_1(E) \right] \cdot 1 \\
&= 2 \cdot \frac{2e^2}{h} \cdot f_1(E)(1 - f_1(E))dE \quad .
\end{aligned}
\tag{5.23}
$$

Note that $\nu = \frac{dI}{e} = \frac{2}{h}dE$ is the frequency of (electron) pulse emission into a channel in the energy range $[E, E + dE]$ and $\langle \Delta a^2 \rangle = e^2 f_1(E) \left[1 - f_1(E) \right]$ is the variance of the (electron) current pulse. Since the current is real, the PSD can be defined unilaterally over the positive frequencies, with a simple factor of 2 accounting for the contributions of the negative frequencies. The total noise current from electrode 1 is

$$
S_{I_1}(\omega = 0) = 2 \frac{2e^2}{h} \int_0^\infty (dE) \frac{1}{e^{(E - \mu_1)/k_B \theta} + 1} \frac{e^{(E - \mu_1)/k_B \theta}}{e^{(E - \mu_1)/k_B \theta} + 1} \quad .
\tag{5.24}
$$

If we introduce a parameter $x = e^{(E - \mu_1)/k_B \theta} + 1$, we obtain

$$
\begin{aligned}
S_{I_1}(\omega = 0) &= 4 G_Q \int_{e^{-\mu_1/k_B \theta} + 1}^\infty (dx) \frac{1}{x^2} k_B \theta \\
&= 4 k_B \theta G_Q \frac{1}{e^{-\mu_1/k_B \theta} + 1} \quad .
\end{aligned}
\tag{5.25}
$$

The total noise current PSD from electrode 2 is identical. The two PSD's add since they are independent. Thus, the total noise current PSD is

$$
S_{I_{tot}}(\omega = 0) = 8 k_B \theta G_Q \frac{1}{e^{-\mu_1/k_B \theta} + 1} \quad .
\tag{5.26}
$$

In the limit $\mu_1 \gg k_B \theta$,

$$
S_{I_{tot}}(\omega = 0) = 4 k_B \theta G \quad ,
\tag{5.27}
$$

where $G = 2G_Q$ is the total conductance including two spins. Thus, we have obtained the Johnson-Nyquist thermal noise, starting with the random partition process based on the Fermi-Dirac distribution function.

The current noise at finite frequency, ω, stems from the beat between the occupied wave packet at energy E and the empty wave packets at energies $E \pm \hbar \omega$ [We will show the mathematical proof for this later].

$$
S_{I_1}(\omega)dE = 2 \cdot \frac{2e^2}{h} f_1(E) \cdot \frac{1}{2} \Big[(1 - f_1(E + \hbar \omega)) + (1 - f_1(E - \hbar \omega)) \Big] dE
\tag{5.28}
$$

We again introduce $x = e^{(E-\mu_1)/k_B\theta}$ and $\alpha = e^{x\hbar\omega/k_B\theta}$ and note that:

$$k_B\theta \int_{e^{-\mu_1/k_B\theta}}^{\infty} (dx) \frac{1}{x+1} \cdot \frac{\alpha}{\alpha x + 1} = k_B\theta \frac{\alpha}{1-\alpha} \left[\ln \frac{\alpha e^{-\mu_1/k_B\theta} + 1}{e^{-\mu_1/k_B\theta} + 1} - \ln \alpha \right] \quad .$$

Using these results, we have the current noise PSD at finite frequency ω:

$$\begin{aligned}
S_{I_1}(\omega) &= k_B\theta G_Q \left[\frac{e^{\hbar\omega/k_B\theta}}{1 - e^{\hbar\omega/k_B\theta}} \cdot \left(\ln \frac{e^{(\hbar\omega-\mu_1)/k_B\theta} + 1}{e^{-\mu_1/k_B\theta} + 1} - \frac{\hbar\omega}{k_B\theta} \right) \right. \\
&\left. + \frac{e^{-\hbar\omega/k_B\theta}}{1 - e^{-\hbar\omega/k_B\theta}} \cdot \left(\ln \frac{e^{-(\hbar\omega+\mu_1)/k_B\theta} + 1}{e^{-\mu_1/k_B\theta} + 1} + \frac{\hbar\omega}{k_B\theta} \right) \right] \quad .
\end{aligned} \tag{5.29}$$

If we look at the regime:

$$\mu_1 \gg \hbar\omega, k_B\theta \Rightarrow \ln \frac{e^{(-\mu_1 \mp \hbar\omega)/k_B\theta} + 1}{e^{-\mu_1/k_B\theta} + 1} \to 0 \quad ,$$

we find that:

$$S_{I_1}(\omega) = 2G_Q \hbar\omega \coth \frac{\hbar\omega}{2k_B\theta} \quad . \tag{5.30}$$

The calculation is identical for the noise current PSD from electrode 2. Since the two noise current PSDs are independent and additive, we have

$$S_{I_{tot}}(\omega) = 2G\hbar\omega \coth \frac{\hbar\omega}{2k_B\theta} \quad . \tag{5.31}$$

Thus, we have the generalized Nyquist noise formula, which reduces to the Johnson-Nyquist thermal noise $4k_B\theta G$ in the limit of $\hbar\omega \ll k_B\theta$ and the quantum zero-point noise $2\hbar\omega G$ in the limit of $\hbar\omega \gg k_B\theta$.

5.2.3 Current Noise at Non-Equilibrium

We now have an applied bias voltage such that, $\mu_2 = \mu_1 - eV$. Following the similar procedure of the previous section, we see that the net current is:

$$I_{tot} = I_1 - I_2 = \frac{2e}{h} \int_0^{\infty} (dE) \left[\frac{1}{e^{(E-\mu_1)/k_B\theta} + 1} - \frac{1}{e^{(E-\mu_1+eV)/k_B\theta} + 1} \right] = \frac{2e^2}{h} V = GV \quad .$$

We recover the main result of Sec. (5.2.1). The current noise PSD is calculated by replacing $f_2(E)$ with theFermi-Dirac distribution function with a chemical potential $\mu_2 = \mu_1 - eV$ in (5.28). Performing the similar integration as that of the previous section, we find the solution is general, and is independent of the bias eV as long as $eV \ll \mu_1$, μ_2. Thus, in this limit, the noise current PSD remains unchanged:

$$S_{I_{tot}}(\omega) = 2G\hbar\omega \coth \frac{\hbar\omega}{2k_B\theta} \quad .$$

From the above discussion, it is clear that at equilibrium, not only the dissipation but also the fluctuations of the mesoscopic system can be associated with the contact reservoirs. This is in sharp contrast to the macroscopic conductor, in which both dissipation and fluctuation are associated with the conductor itself. It is interesting to ask how the transition occurs between these two extreme cases. We will discuss this important issue in the remaining of this chapter.

5.3 Partition Noise in Mesoscopic Conductors

Under nonequilibrium conditions, a net current flows through a device, giving the possibility of additional noise. This is not the case if a mesoscopic conductor has a ballistic transport. In the previous section, we established a very important conclusion: a ballistic conductor with unity transmission coefficient features a generalized Johnson-Nyquist noise even at non-equilibrium situation. However, if a mesoscopic conductor has a scatterer along its path, a new noise source emerges. This noise is partition noise, which can actually be viewed as a general phenomenon in many systems. It refers to the fluctuations arising from the independent, random division of discrete objects – in this case, electrons. It has an essentially classical origin, as the simple probabilistic arguements presented in chapter 1. In other words, the electrons in the branching circuit can be replaced by scattering billiard balls, or even random coin tosses; in all cases, the output statistics are just determined by the binomial distribution.

But rather than appearing in the classical limit of tranport where electrons are considered solely as classical particles, electron partition noise appears only in the mesoscopic regime, where the wave nature manifests. In other words, this partition noise is not observed in a macroscopic conductor. It is a surprising experimental finding that macroscopic conductor features also a generalized Johnson-Nyquist noise at non-equilibrium situation. To understand this, it is useful to treat the partition noise phenomenon within a larger context that takes into account the electron's wave-particle duality. This analysis should therefore simultaneously consider both the amplitude and phase of the electron.

The basis for this kind of treatment lies in the coherent scattering (Landauer-Büttiker) approach, a generalization of the Landauer transmission concept to multiple ports[17]. This theory begins by defining single electron states based on the scattering matrix for the coherent device. For each electron state, partitioning by the scatterer introduces intrinsic quantum fluctuations of the appropriately defined number and phase difference operators for the electron. The fluctuations can be elegantly represented on a Bloch sphere diagram, and satisfy the complementarity imposed by the Heisenberg uncertainty relation[18]. The coupling of vacuum fluctuations through the scattering matrix gives rise to these fluctuations[19, 20], and the full quantum mechanical analysis reveals the importance of vacuum fluctuations for not only the number, but also the phase noise due to partitioning.

5.3.1 Coherent Scattering Theory

The coherent scattering theory for a general device with $\mathcal{P}$ ports is similar to the quantum circuit theory of Chapter 3 and begins by defining the asymptotic states in the ports. Assuming only a lattice potential, and no other interactions, and within the effective mass and independent electron approximations, these states in general are simply plane waves, such as in (5.7). The ports are assumed to be semi-infinite in the longitudinal (along the direction into the device) direction, and bounded in the transverse direction, as shown in Fig. 5.7. The two dimensional problem can be decoupled, giving wavefunctions $\zeta_{\alpha j}(y_\alpha)$ for the jth transverse mode in reservoir α (which has J_α total modes), and a plane wave $\exp(\pm i k_{\alpha j} x_\alpha)$ in the longitudinal directon. The associated energy dispersion relation is given by (5.12). Note that x_α, y_α are the local Cartesian coordinates of reservoir α, and
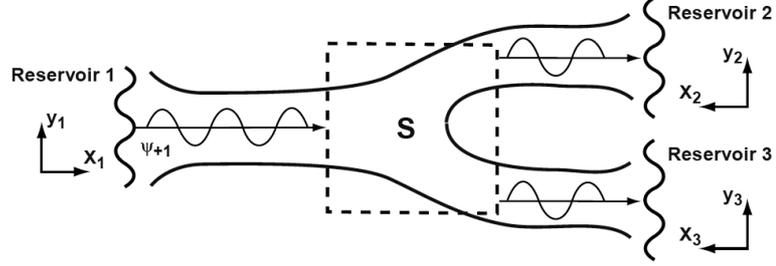
x_α always points into the device.

Figure 5.7: Coherent scattering model. A scattering matrix, **s** couples the plane wave state incident from one reservoir, e. g. ψ_{+1}, with outgoing plane waves in other reservoirs.

Since the device is coherent, a unitary, energy dependent scattering matrix **s** with elements $s_{\beta\alpha ij}(E)$ which couples the incident longitudinal wave with transverse mode j and wavevector $k_{\alpha j}(E)$ in reservoir α to the outgoing longitudinal wave with transverse mode i and wavevector $k_{\beta i}(E)$ in reservoir β can be determined . This matrix can then be used to write the stationary scattering states $\psi_{+\alpha j}(E)$ for longitudinal waves incident on the device from reservoir α and mode j:
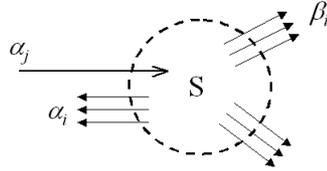
$$\psi_{+\alpha j}(E,x,y) =$$
$$\begin{cases} \sum_{i=1}^{J_\alpha} \left[\delta_{ij}\zeta_{\alpha j}(y_\alpha)e^{ik_{\alpha j}x_\alpha} + \left(\frac{v_{\alpha j}}{v_{\alpha i}}\right)^{\frac{1}{2}} s_{\alpha\alpha ij}\zeta_{\alpha i}(y_\alpha)e^{-ik_{\alpha i}x_\alpha} \right] & (x,y) \in (x_\alpha, y_\alpha) \\ \sum_{i=1}^{J_\beta} \left(\frac{v_{\alpha j}}{v_{\beta i}}\right)^{\frac{1}{2}} s_{\beta\alpha ij}\zeta_{\beta i}(y_\beta)e^{-ik_{\beta i}x_\beta} & (x,y) \in (x_\beta, y_\beta), \beta \neq \alpha \end{cases} ,$$
$$(5.32)$$

where $v_{\alpha j}$ is the (energy-dependent) velocity associated with the $k_{\alpha j}$ plane wave state in reservoir α and mode j. Alternatively, a complete set of outgoing states, $\psi_{-\alpha j}(E)$, instead of incident states can also be defined,

$$\psi_{-\alpha j}(E,x,y) =$$
$$\begin{cases} \sum_{i=1}^{J_\alpha} \left[\left(\frac{v_{\alpha j}}{v_{\alpha i}}\right)^{\frac{1}{2}} s_{\alpha\alpha ji}\zeta_{\alpha i}(y_\alpha)e^{ik_{\alpha i}x_\alpha} + \delta_{ij}\zeta_{\alpha j}(y_\alpha)e^{-ik_{\alpha j}x_\alpha} \right] & (x,y) \in (x_\alpha, y_\alpha) \\ \sum_{i=1}^{J_\beta} \left(\frac{v_{\alpha j}}{v_{\beta i}}\right)^{\frac{1}{2}} s_{\alpha\beta ji}\zeta_{\beta i}(y_\beta)e^{ik_{\beta i}x_\beta} & (x,y) \in (x_\beta, y_\beta), \beta \neq \alpha \end{cases} ,$$
$$(5.33)$$

14
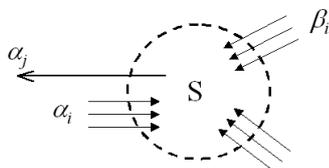
where $s_{\alpha\beta ji}(\mathbf{B}) = s_{\beta\alpha ij}(-\mathbf{B})$ (where $\mathbf{B}$ is the magnetic field) due to time reversal symmetry.

It is convenient to introduce second quantization notation, and associate the ladder operators $\hat{a}_{+\alpha j}(E)$ and $\hat{a}_{-\alpha j}(E)$ with the amplitude of the states $\psi_{+\alpha j}(E)$ and $\psi_{-\alpha j}(E)$, respectively. These operators obey an anticommutation relation,

$$\{\hat{a}^{\dagger}_{\pm\alpha j}(E), \hat{a}_{\pm\beta i}(E')\}_+ = \delta_{\alpha\beta}\delta_{ji}\delta(E - E') \quad . \tag{5.34}$$

Moreover, they are related to each other through the scattering matrix,

$$\hat{a}^{\dagger}_{-\alpha j}(E) = \sum_{\beta=1}^{\mathcal{P}}\sum_{i=1}^{J_\beta} s_{\alpha\beta ji}(E)\hat{a}^{\dagger}_{+\beta i}(E) \quad . \tag{5.35}$$

From this description, it is obvious that an electron in an outgoing state is created from the superposition of incident electrons created in different ports, all coupled through the scattering matrix.

If the variance, $\langle \delta N^2_{-\alpha j}\rangle = \langle \hat{a}^{\dagger}_{-\alpha j}\hat{a}_{-\alpha j}\hat{a}^{\dagger}_{-\alpha j}\hat{a}_{-\alpha j}\rangle - \langle \hat{a}^{\dagger}_{-\alpha j}\hat{a}_{-\alpha j}\rangle^2$, is calculated, terms proportional to $\langle \hat{a}^{\dagger}_{+\beta i}\hat{a}_{+\beta' i'}\hat{a}^{\dagger}_{+\beta' i'}\hat{a}_{+\beta i}\rangle$ appear. Use of the anticommutation relation then explicitly recovers contributions to the noise from the vacuum. In other words, fluctuations in the occupation of the outgoing state are induced by the coupling of the vacuum. From the quantum mechanical point of view, this is the fundamental origin of the partition noise. Notice that this noise is fundamentally different from the fluctuations due to the statistical occupation of the electron state according to a distribution function.

5.3.2 Number–Phase Complementarity

Consider the ideal single mode beam splitter in Fig. 5.8 which equally splits a particle incident from one input port into two output ports. This four-port device can be described by the scattering matrix,

$$\begin{pmatrix} \hat{a}_{-1} \\ \hat{a}_{-2} \\ \hat{a}_{-3} \\ \hat{a}_{-4} \end{pmatrix} = \begin{pmatrix} 0 & & \frac{1}{\sqrt{2}} & \frac{1}{\sqrt{2}} \\ & & -\frac{1}{\sqrt{2}} & \frac{1}{\sqrt{2}} \\ \frac{1}{\sqrt{2}} & -\frac{1}{\sqrt{2}} & & 0 \\ \frac{1}{\sqrt{2}} & \frac{1}{\sqrt{2}} & & \end{pmatrix} \begin{pmatrix} \hat{a}_{+1} \\ \hat{a}_{+2} \\ \hat{a}_{+3} \\ \hat{a}_{+4} \end{pmatrix} \quad . \tag{5.36}$$

A number difference operator, $\mathcal{N}'$, for the difference in outgoing particle number at the output ports 3 ($N_{-3} = \hat{a}^{\dagger}_{-3}\hat{a}_{-3}$) and 4 ($N_{-4} = \hat{a}^{\dagger}_{-4}\hat{a}_{-4}$), is defined by

$$2S'_z = \mathcal{N}' \longleftrightarrow [\hat{a}^{\dagger}_{-3}\hat{a}_{-3} - \hat{a}^{\dagger}_{-4}\hat{a}_{-4}] \quad . \tag{5.37}$$
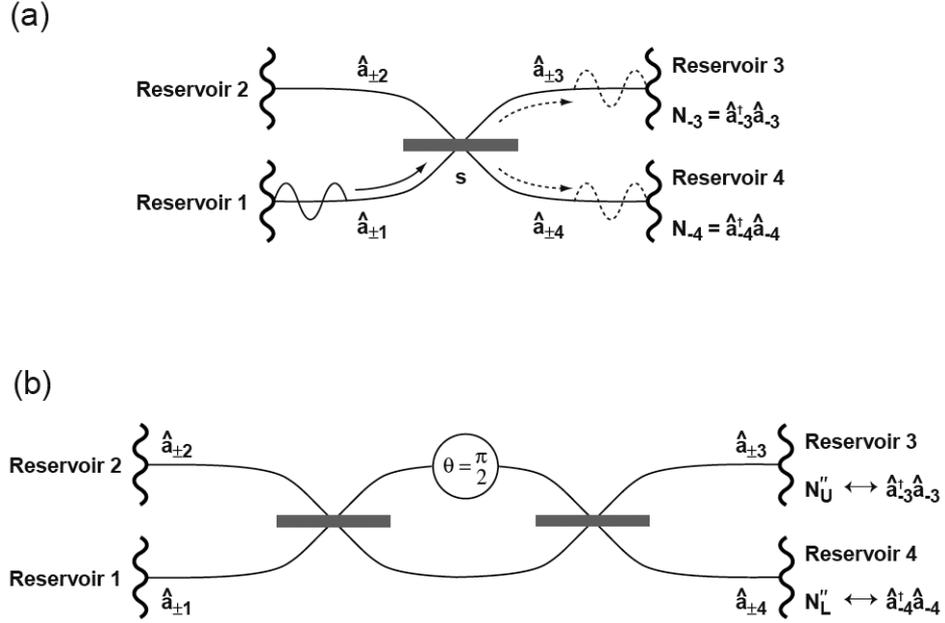
Figure 5.8: (a) An ideal 50-50% electron beam splitter. Operators $\hat{a}_i$ are the second quantized ladder operators for the incident and outgoing states of port i. An incident state from port 1 is split into the two output ports, 3 and 4, where the number operators, $N_{-i}, i = 3, 4$, are used to determine the outgoing particle flux. (b) Interferometer geometry for inferring the phase difference fluctuations induced by the first beam splitter. The output fluxes, $\hat{a}^\dagger_{-3}\hat{a}_{-3}$ and $\hat{a}^\dagger_{-4}\hat{a}_{-4}$ are sensitive to the phase difference, θ, between the two paths.

Here $S' = (S'_\mathrm{x}, S'_\mathrm{y}, S'_\mathrm{z})$ is the collective spin operators, which is often used to describe the assembly of two-level atoms (spin $-\frac{1}{2}$ systems) [21]. This corresponds to a projection of the total spin along the z axis (population difference) of the Bloch sphere, and its average value is clearly indicative of the splitting ratio of the beam splitter in the context of the partitioned system.

Similarly, a relative phase difference operator, Φ', is defined analogous way as the dipole moment operator of the atomic system,

$$\frac{S'_y}{|\langle S'_x \rangle|} = \Phi' \longleftrightarrow \frac{-i[\hat{a}^\dagger_{-3}\hat{a}_{-4} - \hat{a}^\dagger_{-4}\hat{a}_{-3}]}{|\langle [\hat{a}^\dagger_{-3}\hat{a}_{-4} + \hat{a}^\dagger_{-4}\hat{a}_{-3}]\rangle|} \quad . \tag{5.38}$$

When the total spin lies close to the x-axis on the Bloch sphere (which can always be achieved by the proper rotation), this operator corresponds to the azimuthal angle of the spin away from the x-axis.

For the partitioned system, this operator is indicative of the phase difference between the two partial waves in the two outputs of the beam splitter.

By defining number and phase difference in this fashion, the spin commutation relation

immediately establishes a Heisenberg uncertainty relation between these two operators. In other words, a complementarity exists between the fluctuations in relative number and phase difference for the ensemble of single particle split into two ports, and it can be expressed as

$$\langle \delta \mathcal{N}'^2 \rangle \langle \delta \Phi'^2 \rangle \geq 1 \quad . \tag{5.39}$$

The number and phase difference noises arise from the incident vacuum fluctuations. To see this, it is convenient to write the second quantized ladder operators in terms of their quadrature field components, $\hat{a}_{+\alpha} = \hat{a}_{+\alpha c} + i\hat{a}_{+\alpha s}$. Using the anticommutation relations

$$\begin{aligned} \{\hat{a}_{+\alpha c}, \hat{a}_{+\beta c}\}_+ &= \tfrac{1}{2}\delta_{\alpha\beta} \quad , \\ \{\hat{a}_{+\alpha s}, \hat{a}_{+\beta s}\}_+ &= \tfrac{1}{2}\delta_{\alpha\beta} \end{aligned} \tag{5.40}$$

(all other relations being zero), and the beam splitter scattering matrix (5.36), the number and phase difference operators can be expressed as

$$\begin{aligned} \mathcal{N}' &= 2[\hat{a}_{+1c}\hat{a}_{+2s} + \hat{a}_{+2c}\hat{a}_{+1s}] \\ \Phi' &= \tfrac{2i}{\langle \mathcal{N} \rangle}[\hat{a}_{+1c}\hat{a}_{+2c} - \hat{a}_{+2s}\hat{a}_{+1s}] \quad . \end{aligned} \tag{5.41}$$

For the fermion beam splitter, the number difference operator arises from the beating of the quadrature components of the two incident states, while the beating of the in-phase components yields the phase difference operator[20]. Although the explicit form differs from the boson results[22], the number and phase difference noise arising from the partition of a single incident fermion is nonetheless traced back to an interference between the vacuum fluctuations in one input and the occupied state in the other. The vacuum fluctuations are therefore essential for maintaining the Heisenberg uncertainty relation, (5.39).

The number difference noise is first determined from the beam splitter geometry ($\mu_1 > \mu_2 = \mu_3 = \mu_4$ in Fig. 5.8(a)). An average current only flows from the biased input reservoir 1 to the two output reservoirs 3 and 4:

$$\begin{aligned} \langle N_3 \rangle &= \langle N_4 \rangle = -\tfrac{1}{2}\langle N_1 \rangle = -\tfrac{1}{2Bh}(\mu_1 - \mu_2) \\ \langle N_2 \rangle &= 0 \quad . \end{aligned} \tag{5.42}$$

Here $1/B$ is a measurement time interval. The fluctuations are

$$\begin{aligned} \langle \delta N_1^2 \rangle = \langle \delta N_2^2 \rangle &= 0 \\ \langle \delta N_1 \delta N_2 \rangle = \langle \delta N_2 \delta N_1 \rangle &= 0 \\ \langle \delta N_3^2 \rangle &= \tfrac{1}{2}|\langle N_3 \rangle| \\ \langle \delta N_4^2 \rangle &= \tfrac{1}{2}|\langle N_4 \rangle| \\ \langle \delta N_3 \delta N_4 \rangle = \langle \delta N_4 \delta N_3 \rangle &= -\langle \delta N_3^2 \rangle. \end{aligned} \tag{5.43}$$

Notice that the fluctuation in each output reservoir is just half of the full shot noise, as expected from the $T(1 - T)$ dependence of the partition noise at $T = 1/2$. It is now easy to conclude that

$$\delta N_3 = -\delta N_4 \quad . \tag{5.44}$$

Thus the electron streams in the output reservoirs are completely anticorrelated. The physical interpretation of this result is simple. Since the chemical potentials are fixed, the

incident current from reservoir 1 is noiseless. The scattering matrix from (5.36) does not permit a reflected stream back into reservoir 1. Thus $\delta N_1 = 0$. Similarly, $\delta N_2 = 0$, using the fact that no average current flows into reservoir 2. Current conservation requires that $\delta N_1 + \delta N_2 + \delta N_3 + \delta N_4 = 0$, so an increase in reservoir 3 forces a corresponding decrease in reservoir 4. This anticorrelation immediately implies

$$\frac{\langle \delta \mathcal{N}'^2 \rangle}{|\langle \mathcal{N} \rangle|} = \frac{\langle (\delta N_3 - \delta N_4)^2 \rangle}{|\langle N_1 \rangle|} = \frac{\langle \delta N_3^2 \rangle + \langle \delta N_4^2 \rangle - 2\langle \delta N_3 \delta N_4 \rangle}{|\langle N_1 \rangle|} = \frac{4\langle \delta N_3^2 \rangle}{|\langle N_1 \rangle|} = 1 \quad , \quad (5.45)$$

where $\delta \mathcal{N}'$ is the number difference fluctuation of the beam splitter output ports, and $\langle \mathcal{N} \rangle = \langle N_1 \rangle$, the incident electron number. The Poissonian noise that is expected in the ballistic division limit has thus been recovered.
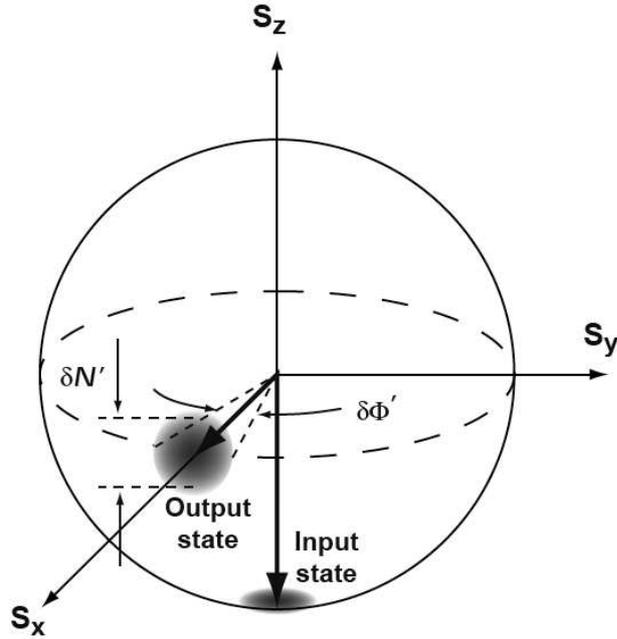

Figure 5.9: Bloch sphere diagram of the input and output spin states of the 50-50 beam splitter. The input state exhibits no number difference noise, $\delta \mathcal{N} = 0$, but has an indeterminate phase. The output state is a coherent spin-state with Poissonian fluctuations in both number ($\delta \mathcal{N}'$) and phase ($\delta \Phi'$) difference.

Next, the phase difference noise is measured by the Mach-Zehnder interferometer, in which the two partial waves propagating along the path 3 and 4 are recombined with a second 50-50% beam splitter after $\pi/2$ relative phase difference (Fig. 5.8 (b)). The average reservoir currents and fluctuations are found to be mathematically identical to the simple beam splitter values due to the $\pi/2$ phase bias. To conserve current, the fluctuations of electron number in reservoirs 3 and 4 are again anticorrelated. Moreover, the statistics of the experiment are again Poissonian. The phase noise is determined by the prescription

given in (5.38), yielding

$$\langle \delta \Phi'^2 \rangle |\langle \mathcal{N} \rangle| = \langle (\delta N_3 - \delta N_4)^2 \rangle / |\langle N_1 \rangle| = 1 \quad . \tag{5.46}$$

Clearly the number and phase difference noise yield the minimum uncertainty product. Moreover, they satisfy this product symmetrically, both producing Poissonian fluctuations. The ballistic electron noise properties do in fact correspond to the coherent spin-state[21] depicted in Fig. 5.9 on the standard Bloch sphere diagram.

5.3.3 Reservoir Currents

In a mesoscopic device, the reservoirs connected to the device ports are sources for many electrons distributed according to the equilibrium Fermi-Dirac distribution. In practice, some energy relaxation mechanism within the reservoirs must exist in order to maintain this distribution in the presence of transport. However, provided there is no reflection from the reservoirs back into the device, the details are unimportant.

To treat all the electrons, many-body scattering states must be defined. Returning now to the general case, the incident states can be superimposed with complex amplitudes to form a general scattering state, from which a field operator can be constructed,

$$\hat{\Psi}(x,y,t) = \sum_{\alpha=1}^{\mathcal{P}} \sum_{j=1}^{J_\alpha} \int \frac{\mathrm{d}E_{\alpha j}}{[h v_{\alpha j}(E_{\alpha j})]^{1/2}} \psi_{+\alpha j}(E_{\alpha j}, x, y) \hat{a}_{+\alpha j}(E_{\alpha j}) e^{-iE_{\alpha j}t/\hbar} \quad . \tag{5.47}$$

A quantum mechanical current operator can be defined to describe the total flux of particles through a reservoir α at some arbitrary longitudinal position x_α,

$$I_\alpha(t) = \frac{e\hbar}{2mi} \int dy_\alpha \left[\hat{\Psi}^\dagger \nabla \hat{\Psi} - (\nabla \hat{\Psi}^\dagger) \hat{\Psi} \right]_{x_\alpha} \quad . \tag{5.48}$$

To compute this, it helps to decompose $\hat{\Psi}$ into a more convenient form which explicitly contains both the incident and outgoing states of α. This is done with the help of (5.35); $\hat{\Psi}(x,y,t)$ can be written for each reservoir α when $(x,y) \in (x_\alpha, y_\alpha)$ as

$$\hat{\Psi}(x,y,t) = \hat{\Psi}(x_\alpha, y_\alpha, t) =$$
$$\sum_{j=1}^{J_\alpha} \int \frac{\mathrm{d}E_{\alpha j}}{[h v_{\alpha j}(E_{\alpha j})]^{1/2}} \zeta_{\alpha j}(y_\alpha) \left[\mathrm{e}^{ik_{\alpha j}x_\alpha} \hat{a}_{+\alpha j}(E_{\alpha j}) + \mathrm{e}^{-ik_{\alpha j}x_\alpha} \hat{a}_{-\alpha j}(E_{\alpha j}) \right] e^{-iE_{\alpha j}t/\hbar} \quad .$$
$$\tag{5.49}$$

In the low frequency limit, Büttiker shows that (5.48) can now be rewritten in the suggestive form[17],

$$I_\alpha(t) = \frac{e}{h} \int \mathrm{d}E \mathrm{d}E' \left[\hat{\mathbf{a}}_{+\alpha}^\dagger(E) \hat{\mathbf{a}}_{+\alpha}(E') - \hat{\mathbf{a}}_{-\alpha}^\dagger(E) \hat{\mathbf{a}}_{-\alpha}(E') \right] \exp \left[i(E - E')t/\hbar \right] \quad , \tag{5.50}$$

where $\hat{\mathbf{a}}_{+\alpha}, \hat{\mathbf{a}}_{-\alpha}$ are vector operators extending over all transverse modes of reservoir α. This emphasizes that the total current in a reservoir is the difference between the incident

currents generated from that reservoir and the outgoing currents induced by the scattering from other reservoirs. In terms of only incident states, this equation can be written as

$$
\begin{aligned}
I_\alpha(t) &= \frac{e}{h} \int \mathrm{d}E \mathrm{d}E' \sum_{\beta=1}^{\mathcal{P}} \sum_{\gamma=1}^{\mathcal{P}} \\
&\times \hat{\mathbf{a}}_{+\beta}^\dagger(E) \left[\mathbf{1}_\alpha \delta_{\alpha\beta} \delta_{\alpha\gamma} - \mathbf{s}_{\alpha\beta}^\dagger(E) \mathbf{s}_{\alpha\gamma}(E') \right] \\
&\times \hat{\mathbf{a}}_{+\gamma}(E') \exp\left[i(E - E')t/\hbar \right] \quad,
\end{aligned}
\tag{5.51}
$$

where $\mathbf{1}_\alpha$ is the $J_\alpha \times J_\alpha$ identity matrix, and $\mathbf{s}_{\alpha\beta}$ is a $J_\beta \times J_\alpha$ matrix representing the scattering from the transverse modes of reservoir β to the transverse modes of reservoir α. This is one of the principle formulas of the coherent scattering theory since it relates the macroscopically measured net current to the microscopic scattering matrix of the electrons.

To determine the current averaged over the reservoir Fermi-Dirac distributions in the presence of different chemical potentials, (5.51) can be used to give

$$
\begin{aligned}
\langle I_\alpha \rangle &= \frac{e}{h} \sum_{\beta=1}^{\mathcal{P}} \int \mathrm{d}E \, \mathrm{Tr} \left[\mathbf{1}_\alpha \delta_{\alpha\beta} - \mathbf{s}_{\alpha\beta}^\dagger(E) \mathbf{s}_{\alpha\beta}(E) \right] f_\beta(E) \\
&= \frac{e}{h} \int \mathrm{d}E \left[(J_\alpha - T_{\alpha\alpha}) f_\alpha(E) - \sum_{\beta\neq\alpha=1}^{\mathcal{P}} T_{\alpha\beta} f_\beta(E) \right] \quad.
\end{aligned}
\tag{5.52}
$$

In this expression, $T_{\alpha\beta} = \mathrm{Tr}\left[\mathbf{s}_{\alpha\beta}^\dagger \mathbf{s}_{\alpha\beta} \right]$ is the transmission probability between reservoirs β and α, and $J_\alpha = \sum_{\beta=1}^{\mathcal{P}} T_{\alpha\beta}$ by unitarity. It is important to emphasize that according to (5.51), only the distribution of electrons incident on the device from each reservoir is needed; the distribution of outgoing electrons is determined by the scattering.

The Fourier transform of (5.51) can be used to determine the low frequency current fluctuations $\delta I_\alpha(\omega) = I_\alpha(\omega) - \langle I_\alpha(\omega) \rangle$, and the unilateral current spectral density, $S_{\delta I_\alpha \delta I_\beta}(\omega)$, measured in a frequency interval $\delta\nu$, is

$$
S_{\delta I_\alpha \delta I_\beta}(\omega)\delta\nu = \langle \delta I_\alpha(\omega) \delta I_\beta(-\omega) + \delta I_\beta(-\omega) \delta I_\alpha(\omega) \rangle \delta\nu \quad.
\tag{5.53}
$$

This is the generalization of the variance of the occupation of a single state, discussed earlier. It is a second order expression in the current, but fourth order in the wavefunction amplitude. In this sense, it is directly analogous to optical intensity-intensity correlations, such as was measured in the experiment by Hanbury Brown and Twiss[23]. A spectral density is now given by

$$
\begin{aligned}
S_{\delta I_\alpha \delta I_\beta}(\omega) &= \frac{e^2}{h} \int \mathrm{d}E \sum_{\gamma=1}^{P} \sum_{\epsilon=1}^{P} \\
&\times \mathrm{Tr}\left[(\mathbf{1}_\alpha \delta_{\alpha\gamma} \delta_{\alpha\epsilon} - \mathbf{s}_{\alpha\gamma}^\dagger(E) \mathbf{s}_{\alpha\epsilon}(E + \hbar\omega))(\mathbf{1}_\beta \delta_{\beta\gamma} \delta_{\beta\epsilon} - \mathbf{s}_{\beta\gamma}^\dagger(E + \hbar\omega) \mathbf{s}_{\beta\epsilon}(E)) \right] \\
&\times \{ f_\gamma(E) \left[1 - f_\epsilon(E + \hbar\omega) \right] + f_\epsilon(E + \hbar\omega) \left[1 - f_\gamma(E) \right] \}
\end{aligned}
\tag{5.54}
$$

Note that at zero temperature and zero frequency, the product of the distributions in $S_{\delta I_\alpha \delta I_\alpha}$ suggests the same vacuum fluctuation interpretation given earlier. That is, a

contribution is made to the noise in reservoir α when one reservoir γ has an occupied state $(f_\gamma(E) = 1)$ while another reservoir ϵ with which it couples into α has a vacuum state $(f_\epsilon(E) = 0)$. This contribution is just the partition noise of that single state. Moreover, since each electron at a different energy is considered independent, (5.54) implies that the total noise is simply a sum over the independent partition noise contributions.

Example: a mesoscopic conductor with a single scatterer.

Now, we introduce a single scatterer into a mesoscopic conductor. The scatterer acts as a second partitioning event, $i.e.$, a second binomiallydistributed process. (The first binomial process is caused by the Fermi-Dirac distribution of the reservoir.) This means that the Fermi-Dirac distribution gives the probability that an electron is injected into the conductor. Conditioned on the event that the electron is successfully injected into the conductor, it is transmitted at the scatterer with probability T. Assume T is independent of an electron energy for a small applied bias voltage.

The average currents become:

$$\langle I_1 \rangle = \frac{2e}{h} \int_0^\infty (dE) \frac{1}{e^{(E-\mu_1)/k_{\mathrm{B}}\theta} + 1} T \quad ,$$

$$\langle I_2 \rangle = \frac{2e}{h} \int_0^\infty (dE) \frac{1}{e^{(E-\mu_2)/k_{\mathrm{B}}\theta} + 1} T \quad .$$

Therefore we have

$$\langle I_{\mathrm{tot}} \rangle = \langle I_1 - I_2 \rangle = 2G_{\mathrm{Q}} V T \quad . \tag{5.55}$$

We consider the zero-frequency current noise PSD in a two-port mesoscopic conductor with a single scatterer. Then, (5.54) has a very simple interpretation. There are two binomial processes in series as mentioned above. To calculate the variance, one would in principle use the Burgess variance theorem. However, the Pauli Exclusion Principle is an additional constraint that must be included in calculating the variance; it adds a complication to the standard Burgess variance theorem.

The standard Burgess variance theorem states that if we have a source (with variance $\sigma(N)$ and average $\overline{N}$) which goes through a partition process with probability T, the noise of the resulting stream is:

$$\sigma_{\mathrm{tot}} = T^2 \cdot \sigma(N) + \overline{N} \cdot T(1 - T)$$

Since the Pauli Exclusion Principle forbids two electrons from sharing the same state,the noise due to the scatterer (binomial partitioning) is seen when only one electron arrives at the scatterer at a time.

In calculating the noise of electrons at electrode 1, we must consider thecontributions from electrons originating at electrode 1 and those originating at electrode 2. Also note that since each mode carriers at most one electron, we are really considering a Bernoulli trial for each electron entry event ($i.e.$, a binomial process of N=1), and later, we integrate over all modes.

   i) Noise at electrode 1 due to electrons from electrode 1

An electron is injected into a mode with energy E with a probability of $f_1(E)$. This electron has a finite chance of being reflected, $R = (1 - T)$. The contribution to the modified Burgess variance theorem is:

$$\sigma_{\text{tot}} = T^2 \cdot f_1(E)\Big(1 - f_1(E)\Big) + f_1(E) \cdot T(1 - T)\Big(1 - f_2(E)\Big) \quad . \tag{5.56}$$

ii) Noise at electrode 1 due to electrons from electrode 2

An electron is injected into a mode with energy E with a probability of $f_2(E)$. This electron has a finite chance of being transmitted to electrode 1. The contribution to the modified Burgess variance theorem is:

$$\sigma_{\text{tot}} = T^2 \cdot f_2(E)\Big(1 - f_2(E)\Big) + f_2(E) \cdot T(1 - T)\Big(1 - f_1(E)\Big) \quad . \tag{5.57}$$

The total noise is given by:

$$
\begin{aligned}
S_{I_1}(\omega) &= 2\frac{2e^2}{h} \cdot \int_0^\infty (dE) \Bigg[T^2 \Big[f_1(E)\Big(1 - f_1(E)\Big) + f_2(E)\Big(1 - f_2(E)\Big) \Big] \\
&\qquad + T(1 - T)\Big[f_1(E)\Big(1 - f_2(E)\Big) + f_2(E)\Big(1 - f_1(E)\Big) \Big] \Bigg] \\
&= 4G_Q \Bigg[2k_B\theta T + 2k_B\theta T(1 - T)\Big[\frac{eV}{2k_B\theta} \coth \frac{eV}{2k_B\theta} - 1 \Big] \Bigg] \\
&= 4k_B\theta GT + 2k_B\theta GT(1 - T)\Big[\frac{eV}{2k_B\theta} \coth \frac{eV}{2k_B\theta} - 1 \Big] \tag{5.58}
\end{aligned}
$$

Here $G = 2G_Q$ is the total conductance. The following are some limiting cases:

i) Near zero bias $k_B\theta \gg eV$

Since

$$\Big[\frac{eV}{2k_B\theta} \coth \frac{eV}{2k_B\theta} - 1 \Big] \to \frac{eV}{2k_B\theta} \cdot \frac{2k_B\theta}{eV} - 1 = 0 \quad ,$$

is satisfied, we have

$$S_{I_1}(\omega = 0) \to 4k_B\theta GT \quad .$$

This is the equilibrium thermal noise corresponding to an effective conductance GT.

ii) At high bias, $k_B\theta \ll eV$

Since

$$\coth \frac{eV}{2k_B\theta} \to 1, \Big[\frac{eV}{2k_B\theta} \coth \frac{eV}{2k_B\theta} - 1 \Big] \to \frac{eV}{2k_B\theta} \quad ,$$

is satisfied, we have

$$S_{I_1}(\omega = 0) \to 4k_B\theta G_Q T + 2eI_{\text{tot}}(1 - T) \quad .$$

This approaches a full shot noise as T approaches 0.

5.3.4 Quantum Point Contact Noise

The previous section discussed in depth the theoretical foundation for noise in coherent mesoscopic devices, with particular attention to the phenomemon of partition noise. In this section, the discussion returns to the mesoscopic regime and shifts to focus on the measurement of partition noise in the simplest mesoscopic device – a quantum point contact (QPC), such as in Fig. 5.10.

Although classical statistics can be used to derive the noise power, as is done in the previous section for a mesoscopic conductor with a single scatterer, the coherent scattering theory can directly give the result including the temperature dependence. This is expressed (assuming an energy independent scattering matrix) by (5.54). At low frequencies compared to $k_B\Theta$, this reduces in the case of the QPC to an equilibrium and non-equilibrium current noise in lead 1 of

$$S^{\text{eq}}_{\delta I_1 \delta I_1}(\omega = 0) \;\; = \;\; 4k_B\Theta \frac{2e^2}{h}\left[J - T_{11}\right] \tag{5.59}$$

$$S^{\text{tr}}_{\delta I_1 \delta I_1}(\omega = 0) \;\; = \;\; 2k_B\Theta \frac{2e^2}{h}\left\{\sum_{\gamma=1}^{2}\sum_{\epsilon=1}^{2}\text{Tr}\left[\mathbf{s}^{\dagger}_{1\gamma}\mathbf{s}_{1\epsilon}\mathbf{s}^{\dagger}_{1\epsilon}\mathbf{s}_{1\gamma}\right]\left(\frac{\tilde{\mu}_{\gamma\epsilon}}{2}\coth\frac{\tilde{\mu}_{\gamma\epsilon}}{2}\right) - J\right\} \tag{5.60}$$

where J is the number of transverse modes in the QPC, $\tilde{\mu}_{\gamma\epsilon} = (\mu_\gamma - \mu_\epsilon)/k_B\Theta$ is a normalized bias voltage and spin degeneracy has been included to double the conductance. Assuming the confinement potential varies adiabatically so that there is no scattering between transverse modes, it can be shown that

$$\text{Tr}\left[\mathbf{s}^{\dagger}_{1\gamma}\mathbf{s}_{1\epsilon}\mathbf{s}^{\dagger}_{1\epsilon}\mathbf{s}_{1\gamma}\right] \;\; = \;\; \sum_{j=1}^{J} T_{1\gamma j}T_{1\epsilon j} \tag{5.61}$$

$$T_{11} \;\; = \;\; \sum_{j=1}^{J} T_{11j} \tag{5.62}$$

where $T_{1\gamma j}$ is the transmission probability from γ to 1 for the jth mode, and $T_{11j} + T_{12j} = 1$ for each j. Then the noise reduces to

$$S^{\text{eq}}_{\delta I_1 \delta I_1} \;\; = \;\; 4k_B\Theta \frac{2e^2}{h}\sum_{j=1}^{J} T_{12j} \tag{5.63}$$

$$S^{\text{tr}}_{\delta I_1 \delta I_1} \;\; = \;\; 4k_B\Theta \frac{2e^2}{h}\sum_{j=1}^{J} T_{12j}(1 - T_{12j})\left[\frac{eV}{2k_B\Theta}\coth\frac{eV}{2k_B\Theta} - 1\right]. \tag{5.64}$$

These are the basic equation for the partition noise of a QPC. At zero temperature, it gives[19],

$$S^{\text{eq}}_{\delta I_1 \delta I_1} \;\; = \;\; 0 \tag{5.65}$$

$$S^{\text{tr}}_{\delta I_1 \delta I_1} \;\; = \;\; 2eV \frac{2e^2}{h}\sum_{j=1}^{J} T_{12j}(1 - T_{12j}) \tag{5.66}$$

which is the same as what would be derived from classical statistics. One of the key features is that as a function of the QPC width, the noise power peaks exactly between

the conductance plateaux where the transmission of the highest mode is $T_{12j} = 1/2$. At the plateaux, all the transmission probabilities are unity, so that the non-equilibrium noise is completely suppressed.
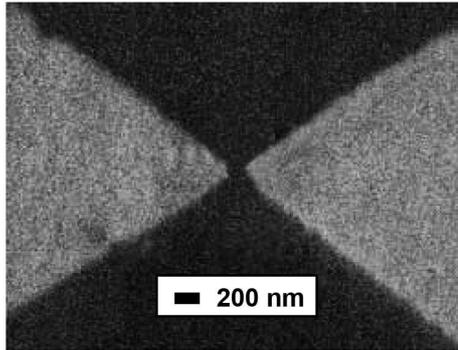

Figure 5.10: SEM photograph of one of the fabricated quantum point contacts (QPC).

The first attempt to observe the noise from a QPC was performed at low frequencies (below 100 kHz) at 4.2 K[24]. The spectrum exhibited primarily a $1/f$ dependence with frequency f, leveling off at higher frequencies. While an oscillatory behavior with gate voltage was observed for the $1/f$ component, it scaled quadratically (not linear) with current. The white noise background at higher frequencies was suppressed from the full shot noise value corresponding to their current biases (0 - 600 nA), but no firm quantitative conclusions were made concerning its origin. Other early attempts to observe the noise spectrum were also restricted to low frequencies, and were sensitive mainly to Random Telegraph Signals (RTS), or switching events in the conductance[25].

More sensitive measurements techniques have since been developed, allowing experiments to truly probe the partition noise regime. Reznikov *et al.* first used an ac modulation technique to measure the noise in a 10 GHz bandwidth[26]. This allowed a discrimination between the device noise, which is modulated, and the background noise due to the amplifier. Clear oscillatory behavior in the noise was observed, but deviations from the theoretical predictions occured below the first plateau. Kumar *et al.* used a cross-correlation technique with two independent amplifiers to reduce the background noise[27]. At low frequencies at dilution refrigerator temperatures, they achieved extremely sensitive noise measurements around the first mode that quantitatively verified the theory.

The results of Liu et al.[28] are shown in Fig. 5.11. Clear peaks in the data are observed in the step regions, while the noise appears to be fully suppressed at the plateau, at least for the first fewtransverse modes. The peak magnitudes against the bias current shows reasonably linear behavior, suggesting that the noise is not due to switching events.

If the data is plotted in the form of Fano factor, the good agreement with theory is obtained. In this case, the assumption is made that the temperature is zero, that the lower modes are fully transmitting, and that only the transmission of the highest mode is changing during a step. This result suggests that little mode mixing – which may add more noise – occurs in the QPC between steps.
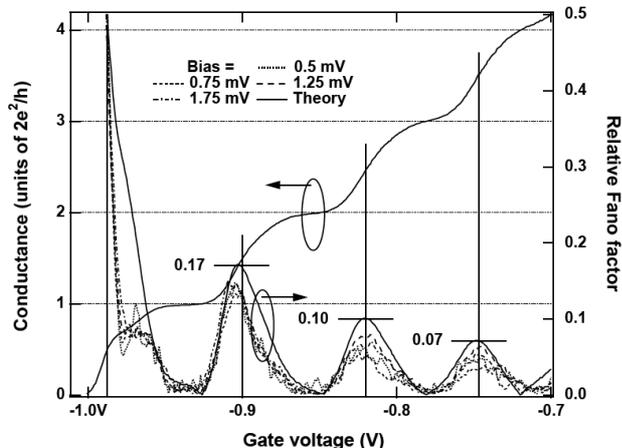
Figure 5.11: The noise power normalized by the noise power at $T = 1/2$ vs. the gate voltage. When renormalized in this fashion, the experimental curves show reasonable agreement with theory.

It is interesting to note that there appears to be a shoulder in the conductance below the first plateau which is associated with a noise reduction far below what would be expected from the transmission. It has been suggested that this shoulder may be a signature of a zero-bias spin splitting in a one-dimensional electron gas[29].

In order to measure the Fano factor of a quantum point contact,the Hanbury-Brown and Twiss interferometer can be employed[23]. In Fig. 5.12(a), we consider the partitioning of particles from a source with Fano factor F_1 at a beam splitter with transmission probability T. The average number of particles transmitted to output 3 is $\langle N_3 \rangle = T \langle N_1 \rangle$. The variance in particle number at output 3 is given by the Burgess variance theorem, $\langle \Delta N_3^2 \rangle = \langle \Delta N_1^2 \rangle T^2 + \langle N_1 \rangle T(1 - T)$ at $\theta = 0$. It follows that the Fano factor at output 3 is $F_3 = TF_1 + (1 - T)$. Between the $(n - 1)$ and n'th conductance plateau, there are $(n - 1)$ channels transmitting with unity probability, and the n'th channel transmitting with probability T_n. In this case, it can be shown that the overall Fano factor is $F^{(n)} = T_n(1 - T_n)/[T_n + (n - 1)]$ at the output of the n-channel QPC.

In principle, one can measure the current noise of a particle source by placing a noise detector immediately after it. This is usually done in mesoscopic systems using a square-law device followed by an averager to get a quantity proportional to the time average of the squared current[26]-[28]. However, a careful calibration is needed to interpret the resulting value, because the transfer function accounting for the noise detection circuit is usually not known *a priori*. One possibility is to put a known noise source in parallel with one's device, but this may hamper the operation of the device. Another possibility is to characterize the detection system without the device, but then adding the device later may change the transfer function.

Another approach is to physically place a beamsplitter after the noise source and calculate the cross-covariance of the output fluxes as shown in Fig. 5.12(a). The normalized

cross-covariance is defined as

$$\rho(\tau) = \frac{\langle \Delta N_2(t) \Delta N_3(t+\tau) \rangle}{\langle \Delta N_2^2 \rangle^{\frac{1}{2}} \langle \Delta N_3^2 \rangle^{\frac{1}{2}}} \quad , \tag{5.67}$$

where τ is the relative delay time between the beamsplitter outputs. By definition, this
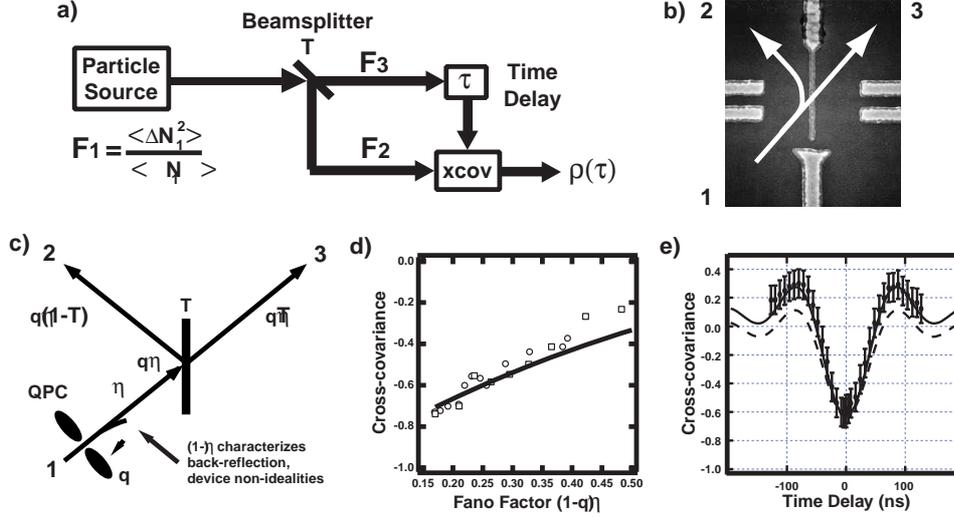

Figure 5.12: a) Cross-covariance schematic. The Fano factor of the source, F_1, can be determined from the cross-covariance, $\rho(\tau)$. b) Device used for the HBT-type intensity interferometer for electrons. Arrows indicate electron entry and partitioning at the electron beamsplitter. c) Probability model for HBT-type intensity interferometer. q is the QPC transmission probability, η accounts for device non-idealities, and T is the beamsplitter transmission probability. d) Cross-covariance *vs.* input Fano factor with $T \approx 0.5$ and $\eta \approx 0.83$. The cross-covariance decreases towards -1 as the Fano factor is reduced towards zero, indicating a quiet source. The solid line is a theoretical trace using equation 5.68. e) Cross-covariance *vs.* delay time at $F = 0.23$. The cross-covariance features a sinc-like behavior due to the finite detection bandwidth (2-10 MHz). A simulation yields the solid line for the actual 2-10 MHz bandwidth, while the dotted line represents a 0-10 MHz lowpass configuration for comparison.

is the cross-correlation of the output fluctuations ΔN_2 and ΔN_3. One can uniquely determine the Fano factor of a source from the cross-covariance for a $T = 0.5$ beamsplitter with zero delay, $\rho(\tau = 0) = (F_1 - 1)/(F_1 + 1)$. In this case, the cross-covariance is positive for $F_1 > 1$ (super-Poisson distributed noise), negative for $0 \leq F_1 < 1$ (sub-Poisson distributed noise), and zero for $F_1 = 1$ (classical, Poisson distributed noise). The advantage of this approach is that, for matched electronics between the two outputs, the transfer function of the experimental detection system is normalized out of the expression. The

positive cross-covariance for photons from a thermal photon reservoir was demonstrated by Hanbury Brown and Twiss[23].

An intensity interferometry with electrons in a 2DEG system is shown in Fig. 5.12(b) [30]. Schottky gates and an etched trench define a four-port device with a narrow, tunable electron beamsplitter. An equivalent transmission probability model is shown in Fig. 5.12(c). The QPC serves as the Fermi-degenerate, single-mode, electron source. In this model, the QPC is ideal with transmission probability $q \in [0, 1]$. Non-idealities, such as coherent back-reflection from the electron beamsplitter, are characterized by the conditional transmission probability, η, which can be experimentally determined. Using this probability model, one can derive an analytic expression for the cross-covariance,

$$\rho(\tau = 0) = \frac{F - 1}{\sqrt{F + \frac{T}{1-T}}\sqrt{F + \frac{1-T}{T}}} = -\left[\frac{q\eta T \cdot q\eta\bar{T}}{(1 - q\eta T)(1 - q\eta\bar{T})}\right]^{\frac{1}{2}} \qquad (5.68)$$

where $F = (1 - q\eta)$ is the Fano factor of the source (including the reservoir, QPC transmission probability, and losses) as seen from the beamsplitter, and $\bar{T} \equiv (1 - T)$. Experimentally, one can vary the Fano factor of the source, F, by tuning the QPC transmission probability, q. The cross-covariance as a function of the Fano factor is plotted in Fig. 5.12(d). As the transmission, q, through the QPC is increased, the Fano factor, F, is decreased, and the input electron flux to the beam splitter carries less (current-normalized) noise. The experimental cross-covariance coefficient approaches -1 as F decreases, in close agreement with the analytical trace calculated using Eq. (5.68). Figure 5.12(e) shows the cross-covariance as a function of the relative delay time, τ, between the two output arms for $F = 0.23$. The sinc-like oscillatory behavior and side-lobe dc-offset are due to the detection bandwidth of the measurement system, 2-10 MHz. The solid line is a zero-parameter fit from a simulation which accounts for the actual detection system including this bandwidth. For comparison, the dashed line is from a simulation using a low pass bandwidth 0-10 MHz which removes the side-lobe dc-offset. A similar result was observed in the edge channel of a GaAs 2DEG in the quantum Hall regime[31].

5.3.5 Electron vs. Photon Noise

Although this section has focused on applying the coherent scattering formalism to an electronic device, it can also be used for a photonic device[17]. In the case of elastic scattering, Büttliker found that the total nonequilibrium noise can depend on the symmetry of the particle's wavefunction. Yet it should be clear from the general discussion above that partition noise is the same regardless of whether electrons or photons are treated since ultimately its quantum mechanical origin is the Heisenberg uncertainty relation, independent of the quantum statistics. To understand whether these statements are consistent or contradictory, it is therefore worthwhile to include a discussion about when and how the symmetry properties of the wavefunction affect the noise.

According to some of the mesoscopic literature, the fermionic nature manifests in the $T(1 - T)$ dependence of the partition noise power; the $f(1 - f)$ dependence is occasionally confused with the $T(1 - T)$ dependence since both T and f enter into the average occupation of an outgoing state. In fact, the Pauli exclusion principle is not a fundamental requirement for observing a $(1 - T)$ dependence of the Fano factor, as is suggested by the fact that it can be derived simply from classical arguments (see Chap. 1).

Consider the beam splitter of (Fig. 5.8) as the prototypical branching circuit for either electrons or photons, and return to the case of single states (rather than reservoirs) incident. It should be clear that if the incident state in port 1 is a fermionic or bosonic number state, $|1\rangle_{+1}$ (with all others being vacuum states), then there are no fluctuations in its number. In other words, the source is quiet. On the other hand, as discussed earlier, the output exhibits partition noise regardless of the symmetry of the wavefunction. For photons, this arguement can be extended to arbitrary definite numbers of photons. A number state is naturally generated by the zero temperature Fermi-Dirac reservoir for a degenerate gas of electrons, so electron partition noise is easily expected.

A practical situation for photons would be to connect the device to a laser or a thermal source. A laser produces light in a coherent state – a superposition over many number states. It exhibits Poissonian fluctuations in intensity. The fluctuations induced on the output by the beam splitting of such a state include contributions from the attenuated Poisson variance and from the partition noise, adding up to again yield the full Poissonian fluctuations. Thus, direct binomial statistics cannot be observed for a laser due to the noise present on the source.

A single state of a reservoir is not necessarily described by a pure number state. It can have occupation fluctuations that are different for fermions and bosons. This is because, unlike Fermi-Dirac statistics, Bose-Einstein statistics has no limitations on the number of particles per state. A straightforward statistical mechanics calculation yields from the distribution function the number fluctuations $\delta N_k = N_k - \langle N_k \rangle$ of a single state k due to thermal energy[32]:

$$\langle \delta N_k^2 \rangle = -k_{\mathrm{B}}\Theta \frac{\partial \langle N_k \rangle}{\partial E_k} \quad , \tag{5.69}$$

where $\langle N_k \rangle = f(E_k)$ for either the Fermi-Dirac orBose-Einstein distributions. Thus, the fluctuations are given by

$$
\begin{array}{rcll}
\langle \delta N_k^2 \rangle_{\mathrm{FD}} & = & f_{\mathrm{FD}}(E_k)\left[1 - f_{\mathrm{FD}}(E_k)\right] & \text{for Fermi} - \text{Dirac statistics} \\
\langle \delta N_k^2 \rangle_{\mathrm{BE}} & = & f_{\mathrm{BE}}(E_k)\left[1 + f_{\mathrm{BE}}(E_k)\right] & \text{for Bose} - \text{Einstein statistics} \\
\langle \delta N_k^2 \rangle_{\mathrm{MB}} & = & f_{\mathrm{MB}}(E_k) & \text{for Maxwell} - \text{Boltzmann statistics} \quad ,
\end{array}
\tag{5.70}
$$

where a zero chemical potential for photons is assumed. It is clear that classical statistics results in Poissonian fluctuations for the occupation of each state, whereas the fermionic statistics result in sub-Poissonian fluctuations (anti-bunching), and bosonic statistics result in super-Poissonian fluctuations (bunching). Obviously, if the state is far below the Fermi energy so that it is fully occupied, it exhibits no fluctuations. But, unless a state is completely unoccupied, all photon states exhibit thermal fluctuations. Thus, the symmetry of the wavefunction clearly plays an important role for the equilibrium fluctuations of the individual reservoir, even before it is connected to a device.

Once connected, quantum statistics continues to play a role in the equilibrium fluctuations. First, the contribution of these equilibrium single state fluctuations to the current noise in any one fermion reservoir α is found from the $\gamma = \epsilon$ terms in (5.54). The fluctuations are attenuated by the transmission probability from γ to α. For the photon reservoir, a similar equation can be derived for the current fluctuations to show the contribution from the attenuated source.

But (5.54) also indicates that there is a contribution to the noise in α at equilibrium from the interference of two different reservoirs, $\gamma \neq \epsilon$. This contribution reflects the quantum statistics in a different way, as can be illustrated again in the case of the 50-50 beam splitter. When one electron is incident along each input port, the antisymmetry of the wavefunction, as it manifests in the Pauli exclusion principle, always forces one electron into each output port, so that there are never any contributions to the fluctuations ($f_\gamma(1 - f_\epsilon) = 1(1 - 1) = 0$ in (5.54). But, if one photon is incident along each input port, then the probability for one photon at each output is exactly zero due to the destructive quantum interference of the bosonic wavefunction. Hence, two photons are always emitted together at one of the output ports or the other, and the number of photons in each output fluctuates.

The main point then is that the equilibrium-like fluctuations can be very different for fermions and bosons because of the quantum statistics. When the reservoirs have different distributions, the transport-like contribution must be added to this to give the total nonequilibrium fluctutations. Whether these transport-like fluctuations depend on the quantum statistics depends on the situation. For fermion partition (at zero temperature), only a single reservoir is biased, and it is clear from the discussion in this section that a $T(1 - T)$ transport contribution arises just from the vacuum fluctuations. This is the same contribution that would arise for single photons, and therefore it is not dependent on the quantum statistics.

The same contribution must also arise for the partitioning of thermal boson reservoirs, although the interpretation is more complicated. Consider the case when one reservoir is set so that the average occupation of all of its states are considerably larger than the occupation at the same energy of the states in the other reservoirs (so that they essentially approximate the vacuum). This would occur if one reservoir is a stellar object and the other reservoir is a cold photodetector. Then there will again be a contribution from partition noise, which has a $T(1 - T)$ dependence. However, it will actually tend to decrease the total fluctuations from the equilibrium fluctuations. The reason is that, as noted above, the equilibrium fluctuations are super-Poissonian due to a bunching of photons into the same state. The partitioning tends to split up these bunches, driving the noise more towards the Poissonian limit.

5.4 Suppression of Mesoscopic Partition Noise

From the previous section, it can be concluded that the nonequilibrium,ballistic division of electrons at a branching circuit such as beam splitter results in intrinsic quantum fluctuations for the number and phase difference operators, and binomial partition noise in a single output current. If a macroscopic conductor is naively considered to consist of many such random scattering events in series, then a natural question arises: Why is partition noise not observed in macroscopic conductors? Indeed, as photons are increasingly scattered, the intensity fluctuations do in fact approach full shot noise.

Previous work on two-port mesoscopic conductors has indicated thatinelastic scattering is important for reaching the macroscopic regime[33]-[35]. In explaining the suppression of electronic shot noise, the literature thus far has emphasized the need for energy dissipation to another system. In this section, the fermionic nature and the role of the Pauli exclusion

principle is strongly emphasized as a key ingredient for explaining why the noise can be suppressed for electrons and not photon[36].

To account for the stochastic nature of inelastic and elastic scatterings, semiclassical Monte Carlosimulations of the noise are presented here[37].

While the scattering of each electron is probabilistic, the scattering outcome is not independent of other electrons. In fact, a correlation is established between individual electrons because of the Pauli exclusion principle. As a result, independent partitioning no longer occurs, and the fluctuations from the scattering can be suppressed. This result is somewhat suggested by the occupation factors in the collision integral E(5.54). The average rate of scattering is reduced by the average occupation of final states. The Monte Carlo simulations allow a dynamic demonstration of this. Moreover, they clarify the feeback mechanism which translates this modulated scattering rate into a suppression of the noise.

Using this algorithm, the predicted one third suppression in the diffusive scattering regime can be recovered. Its origin is attributed to a long time correlation between right and left moving electrons at each position in the channel established by a Pauli exclusion feedback mechanism. Clearly, inelastic scattering is not a necessary ingredient for noise suppression. Second, the initial introduction of distributed inelastic scattering increases the noise, a result which cannot be predicted by the simple scaling argument[33]-[35]. Increased inelastic scattering eventually suppresses the noise by reducing the randomness of the electron distribution in energy. It is this redistribution and not just the energy loss that leads to the further suppression of the partition noise.

5.4.1 Semiclassical Algorithm for Monte-Carlo Simulation

The physical system simulated is a one dimensional conducting channel connected to zero temperature reservoirs at the left and right ends which steadily inject electrons up to their chemical potentials, μ_L and μ_R. A chemical potential bias, $\Delta\mu = eV$, leads to a net electron flux flowing from the left to the right.

For this semiclassical model, individual electrons are represented by wave packets with definite center position and wave number. As shown inFig. 5.13, the full phase space is partitioned into a uniform grid of discrete cells representing distinct single electron states, with each cell (x, k) having a constant width Δx along the position axis and width Δk along the momentum axis. The widths must be chosen so as to give the correct total number of states in the channel, thereby satisfying $\Delta x \Delta k = 1$, which is consistent with the Nyquist sampling theorem for the arrival rate of the degree of freedom and the channel bandwidth. Note that if the total number of states in the channel remains constant, the results should be insensitive to the precise way in which the phase space is divided.

Assuming a free electron dispersion relation in the single transverse mode channel, and given the length of the channel and the applied bias, the total number of cells for right and left moving electrons can be determined. In accordance with the Pauli exclusion principle, each cell can contain only a single electron per spin at any given time. This results in a conductance in the absence of scattering of $2G_Q = 2e^2/h$, where G_Q is the quantum unit of conductance and spin degeneracy is included.

The following assumptions are now made. First, left and right moving cells in the reservoirs whose energies are outside the range μ_L to μ_R are irrelevant to the posed prob-
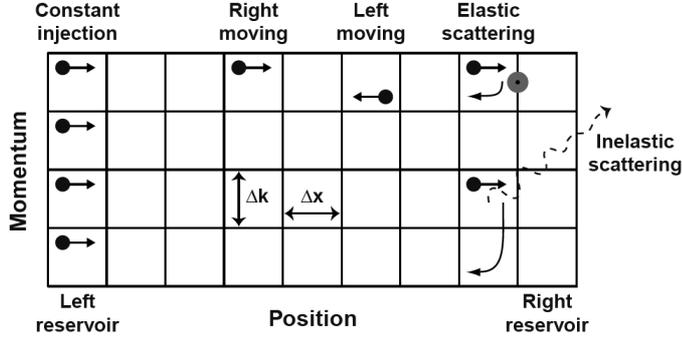
Figure 5.13: Electron phase space in the conductor. The phase space is partitioned into right and left moving electron cells of width Δx by Δk. Elastic scattering reverses the momentum while inelastic scattering also causes a loss in energy.

lem, and are not included in the simulation. Second, the chemical potential bias, $\Delta \mu$, is assumed to be much less than either reservoir chemical potential, allowing the approximation that all electrons move with the same velocity.

In each time step of the simulation, every electron in the channel either moves forward by a single step from (x, k) to $(x + 1, k)$ if $k > 0$, or to $(x - 1, k)$ if $k < 0$, or scatters elastically or inelastically. It is assumed that the simulation time step is short enough that only one scattering event per electron is likely during each time step. At the same time, new electrons are injected into the channel from the biased left reservoir, while electrons at the edges are ejected from the channel.

Distributed elastic scattering induced by the channel boundaries or by a series of tunnel barriers results in a change of state for the electron from cell (x, k) to $(x, -k)$, and is parameterized by a probability r per time step for an electron to intend to elastically scatter, regardless of its position or momentum. In accordance with the Pauli exclusion principle, if another electron moves into the destination state during the same time interval, the scattering will not occur.

The model for inelastic scattering includes only acoustic phonon emission since zero temperature is assumed. Recall that such phonons have a linear dispersion relation, $\omega_q = c_s q$, where ω_q is the frequency of the phonon, c_s is the phonon speed in the material, and q is the phonon wavevector. Requiring that momentum and energy be conserved by the scattering event, it can be shown that the electron momentum reverses direction and decreases by a fixed amount upon scattering $|k_i - k_f| = |q| = 2(|k_i| - mc_s/\hbar)$, where k_i (k_f) is the initial (final) electron wavevector. Thus, the electron at (x, k_i) has a unique state into which it can scatter by this inelastic mechanism. Moreover, the event only occurs if the destination cell (x, k_f) is unoccupied. This process is parameterized by a conditional probability s that the electron intends to inelastically scatter, provided an elastic scattering event is not already likely for that electron. This results in an effective inelastic scattering probability of $s(1 - r)$. The simulation is reasonably insensitive to the order of implementation of the elastic and inelastic scattering.

31

After each time step, the current I_α can be recorded at any position α in the conductor. To obtain the current induced in the leads, the Ramo Theorem can be used and amounts to integrating the current along the entire conductor. However, the dc current at every position is the same since this only depends on whether each electron eventually exits at the right (transmitted) or at the left (reflected). The current fluctuation at high frequencies though is not necessarily the same due to local instantaneous scattering. Nevertheless, for near-dc fluctuations, it is sufficient to consider only the current at one position (which allows for faster simulations).

At the conclusion of the simulation, the spectral density of current fluctuations and correlations between I_α and I_β (where I_α and I_β represent either the net currents at positions α and β, or right and left moving fluxes at the same position) can be calculated according to the formula

$$S_{I_\alpha I_\beta}(\omega) = \frac{2}{\tau} \mathrm{Re} \left\langle \mathcal{I}_\alpha^*(\omega)\mathcal{I}_\beta(\omega) \right\rangle \quad , \tag{5.71}$$

where τ is the total time of the simulation, $\mathcal{I}_\alpha(\omega)$ and $\mathcal{I}_\beta(\omega)$ are the Fast Fourier Transforms of the currents, and the angle brackets indicate an ensemble averaging over many runs of the simulation.

The lowest nonzero frequency that is considered in this discrete simulation is $\omega = 2/\tau \approx 0$, for large τ. The fluctuations S_{II} measured at this frequency are compared with the full shot noise, $2e\langle I\rangle$, in the calculation of the Fano factor, F. In practice, these fluctuations typically vary by less than 10% (usually less than 4% for elastic scattering only) between different positions in the conductor, an indication that the integration time τ is not quite long enough.

Note that the model used here differs from traditional time-of-flight Monte Carlo transport simulations in that it includes the effect of the Pauli exclusion principle on the instantaneous occupation of electron states. Also, it should be remarked that phase coherence between multiple scattering events and Coulomb interactions are ignored.

The values for the adjustable parameters in the simulations have been chosen based on a one dimensional electron gas in GaAs of length $L = 100\mu$m, a Fermi level of $E_F = \mu_2 = 10$ meV, and with a bias of $\Delta\mu = 1$ meV applied between the ends. These yield approximately 210 cells in the channel for both left and right moving electrons. In most simulations, this is divided into 21 wave number levels and 10 positions.

5.4.2 Numerical Results

In Fig. 5.14, the Fano factor is plotted as a function of the conductance of the channel for the various scattering cases. Not only for small elastic scattering but also for small inelastic scattering probabilities, the noise initially increases, a result not predicted using a completely thermalized electron distribution function for the scattered electrons[33]-[35]. An increase would also be expected for photons; it is a consequence of the random scattering process when very few events occur during each time step. Its suppression as compared to the lumped elastic scattering result of $(1-T)$, however, represents the effect of the Pauli exclusion principle.

At higher (distributed) elastic scattering probabilities, the noise is clearly further suppressed. The simulation points can be compared to de Jong and Beenakker's semiclassical
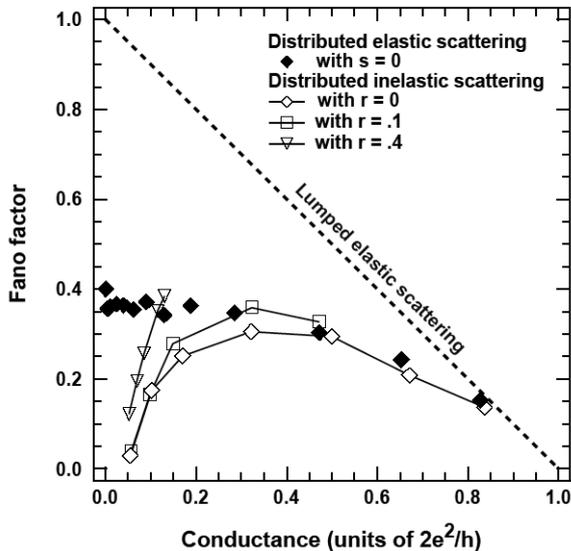
Figure 5.14: The Fano factor for the two-port conductor with distributed elastic and/or inelastic scattering vs. the conductance. The Fano factor is reduced to a level of approximately one third of full shot noise in the case of increasing probability for distributed elastic scattering, r (filled diamonds). This is clearly suppressed as compared to lumped elastic scattering (dashed line). When phonon emissions of energy 50μeV are allowed for $r = 0$ (open diamond), .1 (open square), and .4 (open triangle), the noise is further suppressed.

theory[38] and are found to agree quite well. Inherent in the semiclassical approach is the assumption that the local electron occupation along the conductor is a well defined quantity, even in the case of elastic scattering. It is the fluctuations of this occupation which suppresses the partition noise through a feedback process. The average occupations of the right and left moving cells can be determined from the simulations, and are found to decrease linearly as a function of position along the channel. Consider any position, x, where the current is measured. At some moment in time, due to the random scattering, more electrons are backscattered than on average, resulting in a larger than average number of electrons in the left moving cells at x. The net current therefore decreases. However, because the Pauli exclusion principle restricts the scattering, this excess population will prevent the backscattering of electrons at position $x - 1$. Instead, more electrons will tend to be transmitted to position x. Hence, the net current increases. This is a natural feedback mechanism which suppresses the fluctuations away from the average. Moreover, it should be emphasized that this mechanism is separate from the often quoted one third suppression found from an ensemble average of the $T(1 - T)$ partition noise factor over a bimodal distribution of transmissions. Unlike that coherent scattering result, this mechanism is very sensitive to the distribution of electrons which is consistent with the Pauli exclusion principle.

As shown in Fig. 5.15, evidence for the negative feedback process is provided by the low frequency correlation between the right and left moving fluxes at a position x, $g(\omega) = S_{I_R I_L}(\omega)/\sqrt{S_{I_R I_R}(\omega) S_{I_L I_L}(\omega)}$, where α is now taken to be the right moving flux, and β to be the left moving flux at x in (5.71). For small scattering probabilities, the two fluxes are nearly uncorrelated since backscattering into the nearly unoccupied left moving cells is random. However, as the scattering probability increases, the average left moving flux increases so that regulation of scattering by the Pauli exclusion principle becomes more effective. In this limit, the two fluxes tend towards full correlation, resulting in reduced net current fluctuations.
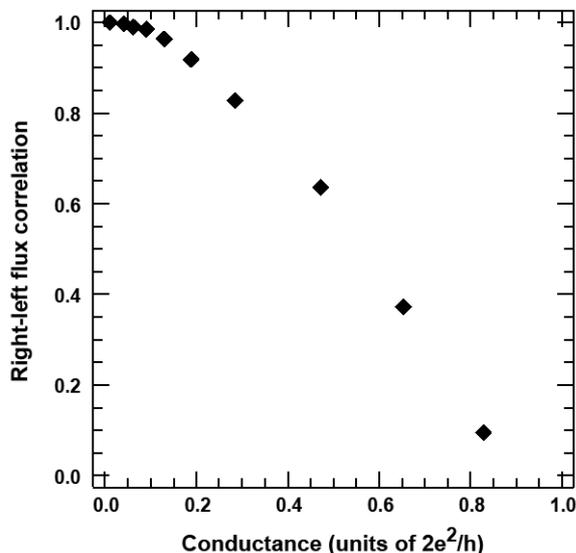

Figure 5.15: The correlation between right and left moving electrons vs. the conductance. The correlation is taken near the two-port conductor's center, and it approaches unity as elastic scattering increases.

The noise is not fully suppressed by elastic scattering alone since the different momentum states are independent. For example, if there is an increase in the total number of right moving electrons at a position, these excess electrons will be distributed randomly among the different momentum states, and will not be able to block an increase of the electron number in other momentum levels. This randomness in energy distribution, as depicted in Fig. 5.16 for the $s = 0$ case, therefore limits the effectiveness of the feedback.

When inelastic scattering is introduced, the different momentum states are coupled, and the energy distribution is driven towards one which exhibits nearly fully occupied low energy states and fully unoccupied high energy states, as is also shown in Fig. 5.16. When s is increased to .9, nearly every electron which does not scatter elastically, will try to scatter inelastically to a lower energy cell if it is available. As a consequence of the Pauli exclusion principle, the result approaches a step-like distribution where the electrons primarily occupy the lower levels.
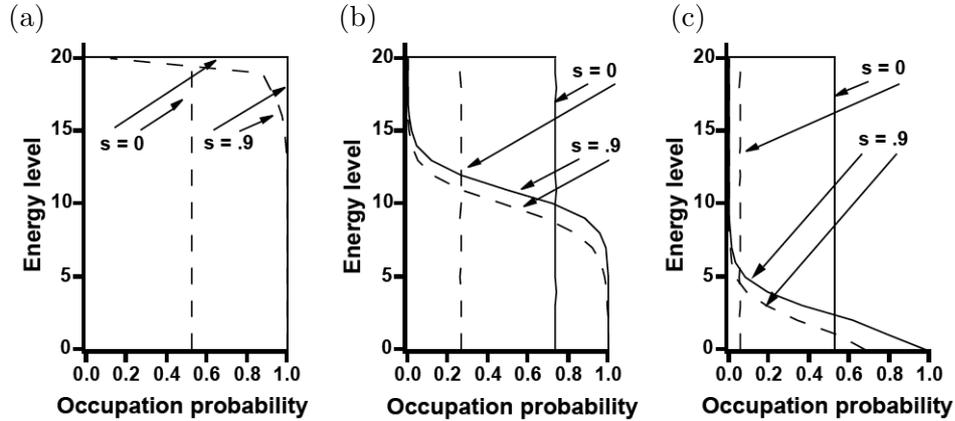
34

Figure 5.16: Electron energy vs. electron occupation at three different positions in the two-port conductor: (a) left, (b) center, (c) right. If the conditional probability for inelastic scattering, s, is zero, then the electrons are equally distributed in energy in both the right moving (solid line) and left moving (dashed line) directions. As s increases to .9, the lower energy states become more fully occupied, while the high energy states become unoccupied.

From this distribution, it is evident that at a given position, the amount of scattering depends on the electron momentum value. Because the occupation is nearly unity for all lower states at the left end, scattering only occurs in the high momentum states. On the other hand, at the right end, almost no scattering occurs at the higher states since there are virtually no electrons. Thus, fluctuations in occupation at a given position are limited only to a narrow range near the transition of the distribution from zero to unity occupation.

The details of the feedback scheme are more complicated now due to the interplay between scattering mechanisms and the coupling of different momentum states. In general though, we expect that if, for example, over a long integration time, the average occupation of a right moving momentum state near the transition increases, then inelastic scattering should tend to "pack" these excess electrons into the lower, left moving cells. If the transition is sharp, these electrons will be less likely to scatter again (elastically or inelastically) to right moving states since these lower energy cells are more likely to be occupied. Hence, the initial increase in right moving electrons is counteracted by an increase in left moving electrons. In this process, inelastic scattering drives the electrons towards a less random distribution. Thus, when occupation fluctuations do occur, inelastic scattering redistributes the electrons into lower momentum states where "Pauli exclusion blockade" is more effective.

5.5 Recovery of Johonson-Nyquit Noise

In studying the nonequilibrium partition noise at zero temperature and frequency in the last three sections, several important points have emerged. First, in the ballistic division regime, partition noise arises as a consequence of the scattering matrix of the device which couples in vacuum fluctuations as the single electron wavefunction is divided into multiple output ports.

In the transition to diffusive and then dissipative transport, the fermionic nature, as manifested by the Pauli exclusion principle, plays an essential role in generating correlations between electrons which suppresses this noise. This is effective first when there is only sparse, random scattering so that the Fano factor for the total nonequilibrium noise increases with decreasing conductance. It is also effective when there is heavy elastic and inelastic scattering, when the Fano factor no longer increases, and can even decrease with decreasing conductance.

In those results, because of the zero temperature and frequency assumptions, there is no contribution to the nonequilibrium noise from the equilibrium-like fluctuations of the reservoirs themselves. In this section, the nonequilibrium noise at finite temperatures and frequencies is considered, and it is shown that in this case, the reservoirs do contribute their equilibrium fluctuations in some way to the total nonequilibrium noise. In fact, as is suggested from the suppression of the zero frequency partition noise, the total nonequilibrium noise in the presence of heavy dissipation is just given by the same generalized Johnson-Nyquist formula, that is used for equilibrium fluctuations, with virtually no contributions from the partition noise induced by the scattering. As mentioned in Chap. 4, this fact has been routinely used in the analysis of noise in macroscopic circuits, but it has not previously been theoretically justified. This section provides this justification (within the independent electron approximation)[39]. Throughout the discussion, an energy-independent scattering matrix and thus a frequency-independent conductance are assumed. Dissipation is introduced by adding purely inelastic scattering reservoirs as ideal voltage probes which are subject to local current conservation. Random inelastic scattering approaches agree with this deterministic reservoir model in the limit of high dissipation.

Recall that the full spectral density of mesoscopic current fluctuations can be derived from the coherent scattering theory, (5.54). If the energy-independence simplification is made, this can be rewritten for finite frequencies as

$$
\begin{aligned}
S_{\delta I_\alpha \delta I_\beta}(\omega) &= S_{\delta I_\beta \delta I_\alpha}(-\omega) = G_Q \sum_{\gamma,\epsilon} \mathrm{Tr}\left[(\mathbf{1}_\alpha \delta_{\alpha\epsilon}\delta_{\alpha\gamma} - \mathbf{s}^\dagger_{\alpha\gamma}\mathbf{s}_{\alpha\epsilon})(\mathbf{1}_\beta \epsilon_{\beta\gamma}\delta_{\beta\epsilon} - \mathbf{s}^\dagger_{\beta\epsilon}\mathbf{s}_{\beta\gamma}) \right] \\
&\times \int dE \left\{ f_\gamma(E)(1 - f_\epsilon(E + \hbar\omega)) + f_\epsilon(E + \hbar\omega)(1 - f_\gamma(E)) \right\} \quad . \quad (5.72)
\end{aligned}
$$

These correlations can be conveniently broken into an equilibrium-like and a transport-like noise contribution, $S_{\delta I_\alpha \delta I_\beta} = S^{\mathrm{tr}}_{\delta I_\alpha \delta I_\beta} + S^{\mathrm{eq}}_{\delta I_\alpha \delta I_\beta}$, each of which independently satisfies a current conservation equation. For any general energy-independent scattering matrix,

$$
\begin{aligned}
S^{\mathrm{eq}}_{\delta I_\alpha \delta I_\alpha}(\omega) &= 4k_B \Theta G_Q \left[J_\alpha - T_{\alpha\alpha} \right] \frac{\tilde{\omega}}{2} \coth \frac{\tilde{\omega}}{2} \qquad\qquad\qquad\qquad (5.73) \\
S^{\mathrm{tr}}_{\delta I_\alpha \delta I_\alpha}(\omega) &= 2k_B \Theta G_Q
\end{aligned}
$$

$$\times \quad \left\{ \sum_{\gamma=1}^{\mathcal{P}} \sum_{\epsilon=1}^{\mathcal{P}} \mathrm{Tr}\left[\mathbf{s}_{\alpha\gamma}^{\dagger}\mathbf{s}_{\alpha\epsilon}\mathbf{s}_{\alpha\epsilon}^{\dagger}\mathbf{s}_{\alpha\gamma}\right] \left(\frac{\tilde{\mu}_{\gamma\epsilon}+\tilde{\omega}}{2}\coth\frac{\tilde{\mu}_{\gamma\epsilon}+\tilde{\omega}}{2}\right) - J_{\alpha}\frac{\tilde{\omega}}{2}\coth\frac{\tilde{\omega}}{2} \right\}$$

(5.74)

$$S_{\delta I_{\alpha}\delta I_{\beta}}^{\mathrm{eq}}(\omega) = -2k_{B}\Theta G_{\mathrm{Q}}\left[T_{\alpha\beta}+T_{\beta\alpha}\right]\frac{\tilde{\omega}}{2}\coth\frac{\tilde{\omega}}{2} \tag{5.75}$$

$$S_{\delta I_{\alpha}\delta I_{\beta}}^{\mathrm{tr}}(\omega) = 2k_{B}\Theta G_{\mathrm{Q}}\sum_{\gamma=1}^{\mathcal{P}}\sum_{\epsilon=1}^{\mathcal{P}}\mathrm{Tr}\left[\mathbf{s}_{\alpha\gamma}^{\dagger}\mathbf{s}_{\alpha\epsilon}\mathbf{s}_{\beta\epsilon}^{\dagger}\mathbf{s}_{\beta\gamma}\right]\left(\frac{\tilde{\mu}_{\gamma\epsilon}+\tilde{\omega}}{2}\coth\frac{\tilde{\mu}_{\gamma\epsilon}+\tilde{\omega}}{2}\right) \quad , \tag{5.76}$$

where $\tilde{\omega} = \hbar\omega/k_{B}\Theta$ and $\tilde{\mu}_{\gamma\epsilon} = (\mu_{\gamma}-\mu_{\epsilon})/k_{B}\Theta$.

The transition from these fluctuations in the coherent division limit to the dissipative limit is modeled through the introduction of purely inelastic scattering reservoirs in the two port device shown in Fig. 5.17. The current in any reservoir can be written in the Langevin form,

$$I_{\alpha} = \frac{e}{h}[\Lambda\mu_{\alpha} - \sum_{\beta\neq\alpha}T_{\alpha\beta}\mu_{\beta}] + \delta I_{\alpha} \quad , \tag{5.77}$$

where $\Lambda_{\alpha} = (J_{\alpha}-T_{\alpha\alpha}) = \sum_{\gamma\neq\alpha}T_{\alpha\gamma}$. Here, δI_{α} represents the intrinsic noise (fluctuating term) when all chemical potentials are held fixed, and it is characterized by the product of the noise bandwidth $\Delta\nu$ and the spectral density, (5.54). In the zero temperature, zero frequency limit, this can be written as

$$\langle \delta I_{\alpha}\delta I_{\beta}\rangle = \frac{2e^{2}\Delta\nu}{h}\sum_{\gamma\epsilon}\int_{0}^{\infty}dE$$
$$\times \quad \mathrm{Tr}\left[(\mathbf{1}_{\alpha}\delta_{\gamma\alpha}\delta_{\epsilon\alpha}-\mathbf{s}_{\alpha\gamma}^{\dagger}\mathbf{s}_{\alpha\epsilon})(\mathbf{1}_{\beta}\delta_{\gamma\beta}\delta_{\epsilon\beta}-\mathbf{s}_{\beta\gamma}^{\dagger}\mathbf{s}_{\beta\epsilon})\right]f_{\gamma}(E)\left[1-f_{\epsilon}(E)\right] \tag{5.78}$$

For the scattering reservoirs to behave realistically as distributed inelastic scatterers, they must not source or sink any current; thermalization cannot result in any gain or loss of electrons. This requirement of local charge conservation is implemented by assuming the scattering reservoirs are connected to the external circuit via infinite impedance leads, essentially becoming voltage probes. Mathematically, this is realized by imposing

$$I_{\mathrm{scat}} \equiv 0 \quad . \tag{5.79}$$

That is, the instantaneous current of the scattering reservoir must vanish so that total current conservation between the input and output reservoirs is preserved.

This results in two sets of linear equations. The set of homogeneous equations,

$$\left\{\frac{h}{e}\langle I_{\gamma}\rangle = \Lambda_{\gamma}\mu_{\gamma} - \sum_{\beta\neq\gamma}T_{\gamma\beta}\mu_{\beta} = 0 \; : \; \gamma = \mathrm{scat}_{1},\dots,\mathrm{scat}_{M}\right\} \quad , \tag{5.80}$$

determines the average chemical potentials that zero the average current.

In addition, since the intrinsic current fluctuations also have to be compensated, the chemical potentials of the scattering reservoirs must also fluctuate. Qualitatively, excess electrons are absorbed by the scattering reservoir and are scattered inelastically. But because they cannot be sunk to ground, they must be reemitted. By assumption, the distribution for reemitted electrons is simply an equilibrium distribution characterized

by a chemical potential. Thus the thermalized electrons can only fill up states near the chemical potential, because of the Pauli exclusion principle. This implies the chemical potential has to fluctuate by an amount $\delta\mu_{\text{scat}}$ determined from the solution to a set of inhomogeneous linear equations,

$$\left\{ \frac{h}{e}\Delta I_\gamma = \Lambda_\gamma \delta\mu_\gamma - \sum_{\beta \neq \gamma} T_{\gamma\beta}\delta\mu_\beta + \frac{h}{e}\delta I_\gamma = 0 \ : \ \gamma = \text{scat}_1, \ldots, \text{scat}_M \right\} \quad . \tag{5.81}$$

Clearly, $\delta\mu_\gamma$ is a function of the intrinsic current fluctuations in the M scattering reservoirs $(\delta I_{\text{scat}_1}, \ldots, \delta I_{\text{scat}_M})$ which exist when instantaneous local charge conservation is not enforced.

As is shown below, this procedure has two effects. The first is attenuate the average current, as expected for inelastic scattering. The second is to reduce the total current fluctuations associated with the partition due to a correlated, compensating chemical potential fluctuation in the scattering reservoir.
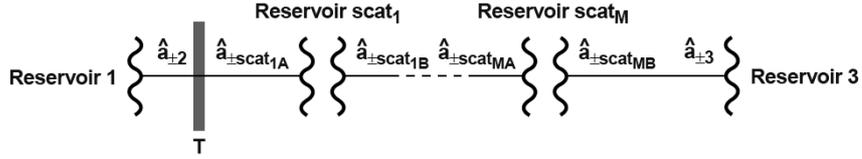

Figure 5.17: A two-port conductor with an elastic scatterer having a finite transmission probability, T. M purely inelastic scattering voltage probes are added after the scatterer.

In the case of finite temperature and frequency, however, the intrinsic fluctuations, $\delta I_{\text{scat}_\gamma}$ are not identically zero, but are rather given by (5.73) and (5.74). Thus, the total current fluctuations, ΔI_3, in the receiving reservoir of a two-terminal device with elastic transmission T are

$$
\begin{aligned}
\Delta I_3 &= \delta I_3 - T_{3\text{scat}_M} G_{\text{Q}} \delta\mu_{\text{scat}_M} \\
&= \delta I_3 + \frac{1}{TM+1} \sum_{\gamma=1}^{M} (1 + (\gamma-1)T)\delta I_{\text{scat}_M}
\end{aligned}
\tag{5.82}
$$

where $T_{3\text{scat}_M}$ is the transmission probability to receiving reservoir 3 from the adjacent scattering reservoir scat_M which has a chemical potential fluctuation $\delta\mu_{\text{scat}_M}$.

To determine $S_{\Delta I_3 \Delta I_3}$, note that the intrinsic current noise of each scattering reservoir is correlated only with the noise of adjacent reservoirs, and that the only nonzero intrinsic transport noise is $S^{\text{tr}}_{\delta I_{\text{scat}_1} \delta I_{\text{scat}_1}}$. Using (5.73) and (5.75) in (5.77) and performing the summations results in

$$S_{\Delta I_3 \Delta I_3}(\omega) = \frac{1}{(TM+1)^2} S^{\text{tr}}_{\delta I_{\text{scat}_1} \delta I_{\text{scat}_1}}(\omega) + 4k_B\Theta \frac{TG_{\text{Q}}}{TM+1} \frac{\tilde{\omega}}{2} \coth\frac{\tilde{\omega}}{2} \tag{5.83}$$

where

$$
\begin{aligned}
S^{\mathrm{tr}}_{\delta I_{\mathrm{scat}_1} \delta I_{\mathrm{scat}_1}}(\omega) \;=\;& 2k_B \Theta T G_{\mathrm{Q}} (1 - T) \\
\times\; & \left[\frac{\tilde{\omega} + \tilde{\mu}_M}{2} \coth \frac{\tilde{\omega} + \tilde{\mu}_M}{2} + \frac{\tilde{\omega} - \tilde{\mu}_M}{2} \coth \frac{\tilde{\omega} - \tilde{\mu}_M}{2} - 2\frac{\tilde{\omega}}{2} \coth \frac{\tilde{\omega}}{2} \right] \;,
\end{aligned}
\tag{5.84}
$$

and $\tilde{\mu}_M = \tilde{\mu}/(TM + 1)$.

The physical content of these equations can be understood as follows. Because of dissipation in the inelastic scattering reservoirs, each additional ideal voltage probe decreases the channel's conductance. For general M, the two-port device has an output conductance of $G_{\mathrm{TT}} = TG_{\mathrm{Q}}/(TM + 1)$.

Because of the local current conservation restriction, the total noise contributed by this dissipation to the receiving reservoir noise is represented by $-T_{3\mathrm{scat}_M} G_{\mathrm{Q}} \delta\mu_{\mathrm{scat}_M}$. Apparently, (5.82) suggests that the contribution of the earliest inelastic scattering, $\delta I_{\mathrm{scat}_1}$, to the current noise, ΔI_3, is reduced by roughly a factor of $1/M$ for large M. The contribution from each following reservoir to $\delta\mu_{\mathrm{scat}_M}$ is increased until the last scattering reservoir is virtually unsuppressed. Consequently, the high frequency noise stems from the vacuum fluctuations and the low frequency noise stems from the thermal Fermi-Dirac fluctuations contributed by all the scattering reservoirs. That is, it originates from channel dissipation rather than from the input and output reservoirs, as in the case of ballistic transport.

This coherent scattering formalism yields the generalized Johnson-Nyquist noise for the nonequilibrium case in the heavily dissipative limit. This is the desired result. To characterize this noise, the spectral densities can be normalized by the dc thermal noise $4k_B\Theta G$ where G is either $2G_{\mathrm{BS}}$ or G_{TT}. The suppression of nonequilibrium noise is shown in Fig. 5.18 for the beam splitter geometry for a frequency of 1 kHz, and a temperature of about 50 mK. For small biases, below the thermal voltage, the total noise is dominated by the thermal noise. For $M = 0$, and voltages larger than the thermal voltage, partition noise dominates. As is depicted, the above equations indicate that this partition noise is suppressed by a factor of $1/(M+1)$ for the beam splitter, and $1/(TM+1)$ for the two-port device, as M increases. As in the zero frequency case, this suppression occurs because any initial elastic scattering near the biased input reservoir is irrelevant for the output reservoir noise if sufficient inelastic scattering occurs to force the electron to the Fermi surface. In other words, the chemical potential fluctuations near the elastic scattering may be large due to the excess noise, but are reduced by the time they reach the output reservoir because of a smoothing effect from the inelastic scattering.

The noise spectrum is plotted in Fig. 5.19 for the two port device (with $T = R = 1/2$). A temperature of 50 mK and a bias of 2.5 mV ($eV/k_B\Theta = 602$, giving a 100 nA current across G_{Q}) are assumed.

It should be noted that there is a transition from the partition noise at finite but low frequency to the quantum noise at high frequency. Both regions, though, can be understood as arising from vacuum fluctuations. At low frequencies, the energies of the occupied electron states which interfere with the vacuum generally lie only within eV of the lowest Fermi level. This is partition noise. At high frequencies, the energy range can extend further, and is limited by $h\nu$ rather than eV. This is the quantum noise region, and it has contributions not only from the electron states and vacuum states of the same

Beam splitter, T = R = 0.5

10^3

Normalized output noise power

10^2

M=0
M=1
M=4

Ballistic

10

M=20

Equilibrium
noise regime

1

Dissipative

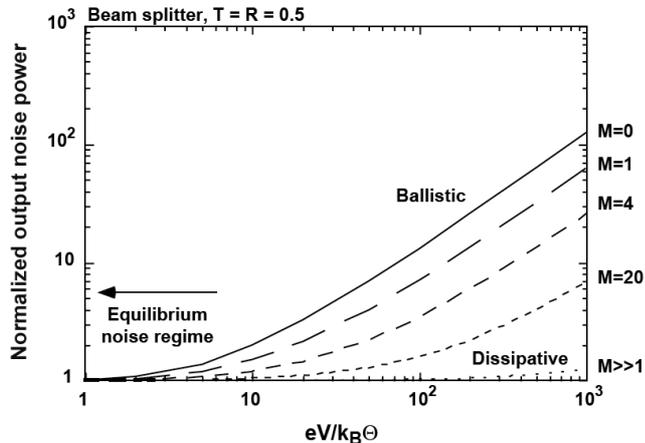M>>1

1   10 10^2 10^3

$eV/k_B\Theta$

Figure 5.18: The current noise at 1 kHz (normalized to the generalized Johnson-Nyquist noise with a conductance of $G_Q/(M+1)$) vs. the voltage bias normalized by the thermal voltage, $k_B\Theta/e$. As inelastic scattering increases (increasing M), the transport noise is suppressed to the generalized Johnson-Nyquist noise limit.

reservoir, but also from different reservoirs. This transition between partition noise and quantum noise has been observed in a diffusive, metallic conductor at high frequencies[40].

To conclude this theoretical discussion of the nonequilibrium noise in the mesoscopic to macroscopic transition, it is useful to review the basic results. Table 5.1 summarizes the low frequency limits of the noise for a two-port conductor in various cases. It divides this into two regimes – the left column corresponds to the case when the applied voltage is much less than the thermal voltage (equilibrium limit), and the right column to the opposite extreme (nonequilibrium limit). It is not surprising that the noise can be different in these two cases since as has been repeatedly stressed, there are fundamentally two kinds of noise. The first stems from the fluctuations of the reservoirs themselves, and the second is associated with the scattering due to the device.

When the transport is completely ballistic, with $T = 1$, the noise in both regimes is just given by $4k_B\Theta G$, where $G = 2G_Q$. There is no noise due to the scattering, so partition noise is absent. However, if there is a non-unity transmission due to finite elastic scattering, then partition noise, $2eVGT(1 - T)$ appears, and can be much larger than the equilibrium fluctuation. In this limit of $T \to 0$, this partition noise approaches a full shot noise. At equilibrium limit, the current noise is given by the thermal noise with the conductance GT.

In the limit of diffusive transport with heavy distributed elastic scattering, the conductance is further reduced. Close to equilibrium, the total noise is still given by the thermal noise formula, with the reduced conductance G. However, under nonequilibrium conditions, the noise is dominated by the scattering, but its magnitude can be suppressed to one-third of full shot noise noise. The origin of this suppression is associated with the
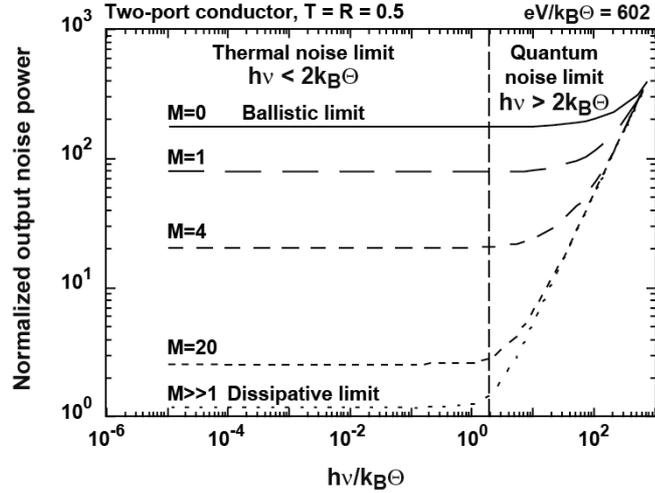
Figure 5.19: The current noise (normalized to the Johnson thermal noise with a conductance of $TG_Q/(TM+1)$) for a two-terminal device with elastic transmission $T = 0.5$ vs. the frequency normalized by the thermal frequency. The transport noise is again suppressed to the genealized Johnson-Nyquist noise limit by increasing M.

Pauli exclusion principle. If electron-electron scattering is taken into account, the noise suppression factor is no more universal $1/3$ but depends on the microscopic details of the scatterings and dimensionality of the system. The Fano factor is roughly

$$F = \begin{cases} 0.7 & d = 1 \\ 1/2 & d = 2 \\ 1/3 & d = 3 \end{cases} \quad . \tag{5.85}$$

The comprehensive review of such a non-degenerate diffusive conductor is given by Blanter and Büttliker[41].

In the limit of dissipative transport with heavy distributed inelastic scattering, the noise due to scattering can be completely suppressed. In the case of large applied biases, only the thermal noise corresponding to the dissipative conductance, G is observed. This is the regime of macroscopic transport. In this case, the Pauli exclusion feedback mechanism to suppress the partition noise is made further effective through the energy dissipation to another system, allowing for a reduction of the randomness of the electron distribution. Clearly, correlations associated with the quantum statistical nature of the electron are at the heart of the noise behavior in the transition from ballistic to dissipative partitioning.

		Equilibrium $V \ll V_{\mathrm{T}}$	Non-equilibrium $V \gg V_{\mathrm{T}}$
Ballistic	no scattering	$4k_{\mathrm{B}}\theta G$	$4k_{\mathrm{B}}\theta G$
	finite elastic scattering	$4k_{\mathrm{B}}\theta TG$	$2eVGT(1-T) = 2e\overline{I}(1-T)$
Diffusive	(distributed elastic)	$4k_{\mathrm{B}}\theta G$	$\frac{2}{3}eVG = \frac{1}{3} \times 2e\overline{I}$
Diffusive	(distributed elastic, Coulomb interaction)	$4k_{\mathrm{B}}\theta G$	$0.7 \times 2e\overline{I}$
Dissipative	(distributed inelastic)	$4k_{\mathrm{B}}\theta G$	$4k_{\mathrm{B}}\theta G$

Table 5.1: Summary of the nonequilibrium noise in various scattering regimes.

Bibliography

[1] R. Dingle, H. L. Störmer, A. C. Gossard, and W. Wiegmann, *Appl. Phys. Lett.* **33**, 665 (1978).

[2] C. Weisbuch and B. Vinter, *Quantum Semiconductor Structures*, (Academic Press, Inc., New York, 1991).

[3] N. W. Ashcroft and N. D. Mermin, *Solid State Physics*, (Saunders College, Philadelphia, 1976), p. 133.

[4] B. K. Ridley, *Quantum Processes in Semiconductors*, (Clarendon Press, Oxford, 1988), p. 28.

[5] G. Bastard, *Wave Mechanics Applied to Semiconductor Heterostructures*, (Les Editions de Physique, Les Ulis, France, 1988).

[6] B. K. Ridley, *Quantum Processes in Semiconductors*, (Clarendon Press, Oxford, 1988), p. 44.

[7] S. Datta, *Quantum Phenomena*, (Addison-Wesley, Menlo Park, CA, 1989).

[8] N. W. Ashcroft and N. D. Mermin, *Solid State Physics*, (Saunders College, Philadelphia, 1976), ch. 12.

[9] B. K. Ridley, *Quantum Processes in Semiconductors*, (Clarendon Press, Oxford, 1988), p. 47.

[10] R. Landauer, *Philosophical Magazine* **21**, 863 (1970).

[11] A. Szafer, A. D. Stone, *Phys. Rev. Lett.* **62**, 300 (1989).

[12] B. J. van Wees, H. van Houten, C. Beenakker, J. G. Williamson, L. P. Kouwenhoven, D. van der Marel, and C. T. Foxon, *Phys. Rev. Lett.* **60**, 848 (1988).

[13] D. A. Wharam, T. J Thornton, R. Newbury, M. Pepper, H. Ahmed, J. Frost, D. G. Hasko, D. C. Peacock, D. A. Ritchie, and G. Jones, *Journal of Physics C: Solid State Physics* **21**, L209 (1988).

[14] S. Datta, *Electronic Transport in Mesoscopic Systems*, (Cambridge University Press, Cambridge, 1995).

[15] W. Bernard and H. B. Callen, *Review of Modern Physics* **31**, 1017 (1959).

[16] R. Landauer, *Physica D* **38**, 226 (1989).

[17] M. Büttiker, *Phys. Rev. B* **46**, 12485 (1992).

[18] R. C. Liu and Y. Yamamoto, *Phys. Rev. B* **49**, 10520 (1994).

[19] G. B. Lesovik, *JETP Lett.* **49**, 592 (1989).

[20] B. Yurke and G. P. Kochanski, *Phys. Rev. B* **41**, 8184 (1990).

[21] F. T. Arecchi, E. Courtens, R. Gilmore, and H. Thomas, *Phys. Rev. A* **6**, 2211 (1972).

[22] C. Caves, *Phys. Rev. D* **23**, 1693 (1981).

[23] R. H. Brown and R. Q. Twiss, *Nature* **177**, 27 (1956).

[24] Y. P. Li, D. C. Tsui, J. J. Heremans, J. A. Simmons, and G. W. Weimann, *Appl. Phys. Lett.* **57**, 774 (1990).

[25] C. Dekker, A. J. Scholten, F. Liefrink, R. Eppenga, H. van Houten, and C. T. Foxon, *Phys. Rev. Lett.* **66**, 2148 (1991).

[26] M. Reznikov, M. Heiblum, H. Shtrikman, and D. Mahalu, *Phys. Rev. Lett.* **75**, 3340 (1995).

[27] A. Kumar, L. Saminadayar, D. C. Glattli, Y. Jin, and B. Etienne, *Phys. Rev. Lett.* **76**, 2778 (1995).

[28] R. C. Liu, B. Odom, Y. Yamamoto, and S. Tarucha, *Nature* **391**, 263 (1998).

[29] K. J. Thomas, J. T. Nicholls, M. Y. Simmons, M. Pepper, D. R. Mace, and D. A. Ritchie, *Phys. Rev. Lett.* **77**, 135 (1996).

[30] W. D. Oliver, J. Kim, R. C. Liu, and Y. Yamamoto, *Science* **284**, 299 (1999).

[31] M. Henny, S. Oberholzer, C. Strunk, T. Heinzel, K. Ensslin, M. Holland, and C. Schönenberge, *Science* **284**, 296 (1999).

[32] F. Reif, *Fundamentals of Statistical and Thermal Physics*, (McGraw-Hill, New York, 1965).

[33] A. Shimizu and M. Ueda, *Phys. Rev. Lett.* **69**, 1403 (1992).

[34] C. W. J. Beenakker and M. Büttiker, *Phys. Rev. B* **46**, 1889 (1992).

[35] R. Landauer, *Phys. Rev. B* **47**, 16427 (1993).

[36] R. C. Liu and Y. Yamamoto, *Physica B* **210**, 37 (1995).

[37] R. C. Liu, P. Eastman, and Y. Yamamoto, *Solid State Communications* **102**, 785 (1997).

[38] M. J. M. de Jong and C. W. J. Beenakker, *Phys. Rev. B* **46**, 13400 (1992).

[39] R. C. Liu and Y. Yamamoto, *Phys. Rev. B* **50**, 17411 (1994).

[40] R. J. Schoelkopf, P. J. Burke, A. A. Kozhevnikov, D. E. Prober, and M. J. Rooks, *Phys. Rev. Lett.* **78**, 3370 (1997).

[41] Ya. M. Blanter and M. Büttiker, *Phys. Rep.* **336**, 1 (2000).